MUSCOVITE $^{40}Ar/^{39}Ar$ GEOCHRONOLOGY OF THE WESTERN PARRY SOUND AND BRITT DOMAINS, CENTRAL GNEISS BELT, GRENVILLE PROVINCE

Kenneth Joseph McKenzie

Submitted in Partial Fulfillment of the Requirements
for the Degree of Bachelor of Science, Honours,
Dalhousie University, Halifax, Nova Scotia
March 1991

Dalhousie University

Department of Geology
Halifax, Nova Scotia
Canada B3H 3J5
(902) 494-2358

DATE May 1, 1991.

AUTHOR Kenneth Joseph McKenzie

TITLE Muscovite $^{40}Ar/^{39}Ar$ Geochronology of the Western Parry Sound and Britt Domains, Central Gneiss Belt, Grenville Province

Degree B.Sc. (Honours) Convocation Spring Year 1991

Distribution License

DalSpace requires agreement to this non-exclusive distribution license before your item can appear on DalSpace.

NON-EXCLUSIVE DISTRIBUTION LICENSE

You (the author(s) or copyright owner) grant to Dalhousie University the non-exclusive right to reproduce and distribute your submission worldwide in any medium.

You agree that Dalhousie University may, without changing the content, reformat the submission for the purpose of preservation.

You also agree that Dalhousie University may keep more than one copy of this submission for purposes of security, back-up and preservation.

You agree that the submission is your original work, and that you have the right to grant the rights contained in this license. You also agree that your submission does not, to the best of your knowledge, infringe upon anyone's copyright.

If the submission contains material for which you do not hold copyright, you agree that you have obtained the unrestricted permission of the copyright owner to grant Dalhousie University the rights required by this license, and that such third-party owned material is clearly identified and acknowledged within the text or content of the submission.

If the submission is based upon work that has been sponsored or supported by an agency or organization other than Dalhousie University, you assert that you have fulfilled any right of review or other obligations required by such contract or agreement.

Dalhousie University will clearly identify your name(s) as the author(s) or owner(s) of the submission, and will not make any alteration to the content of the files that you have submitted.

If you have questions regarding this license please contact the repository manager at dalspace@dal.ca.

Grant the distribution license by signing and dating below.

_____ _____

Name of signatory Date

Muscovite $^{40}Ar/^{39}Ar$ Geochronology of the W. Parry Sound & Britt Domains, C.G.B., Grenville Province

ABSTRACT

$^{40}Ar/^{39}Ar$ analysis of ten muscovite samples from the western Central Gneiss Belt, Grenville Province, Ontario, yielded good argon spectra. The ages calculated show a trend of decreasing age southward into the orogenic interior. These new ages necessitate reinterpretation of previous data from the same area. Combined, the two data sets show an age gradient of -0.23 Ma / km along an 85 km transect through the Britt Domain and northern Parry Sound Domain, perpendicular to the strike of the orogen.

The samples reached muscovite closure temperature more than 70 Ma after deformation ceased. The data record events in the post-tectonic thermal history occurring during the erosional degeneration of the mountain belt.

Two models of post-tectonic thermal behaviour offer possible explanations of this trend in ages. One model assumes erosion-controlled variable uplift rates and a constant geothermal gradient across the transect. The northern end of the transect experiences rapid uplift relative to the south. A greater erosion rate at the margin of the orogen could explain this.

The second model assumes a variable geothermal gradient and constant uplift rate across the transect. The northern end passes through the depressed end of the muscovite closure temperature isotherm first.

A combination of both models may best explain the observed trend in ages.

Key Words: Grenville Province, Central Gneiss Belt, orogen, uplift, geothermal gradient, argon, geochronology, muscovite, radiogenic, closure temperature, plateau

ACKNOWLEDGEMENTS

The author wishes to acknowledge the following people for their assistance during the course of this project:
Dr. Nick Culshaw for field work, introduction to the Grenville and the problem behind this project, collection of many of the samples, and guidance and assistance throughout.
Dr. Peter Reynolds for education and assistance with the theory and techniques of the argon lab.
Dr. D.B. Clarke for direction of the writing and constructive criticism throughout.
Gordon Check for the use of some of his samples and data.
Gordon Brown for preparation of thin sections.
Keith Taylor for instruction in sample preparation and assistance in running the mass spectrometer.
Sandy Grist for help in the mineral separation lab.
Peter Wallace, David Corrigan, and Steven Hinds for collecting several of the samples.
Stephen Rankin for assistance with the petrography.
Melanie Haggart for advice and insight on the use of muscovites as geochronometers.
Cathy Williams, Darren Wheaton, and Kevin DesRoches for assistance with drafting and final assembly.
The other members of the Dalhousie University Department of Geology, especially the Class of 1991, for their help with the little things all year long.

TABLE OF CONTENTS

TABLE OF FIGURES

TABLE OF TABLES

CHAPTER 1: INTRODUCTION

1.1 The Study Area and Its Geology

The Central Gneiss Belt, Georgian Bay, Ontario, lies in the westernmost extent of the Grenville Province, the youngest structural province of the Canadian Shield (Davidson 1984a). The Grenville Province is "a terrane of high grade and structurally complex gneissic rocks" (Davidson 1984a, p 263). It stretches 1900 km from the east coast of Labrador to the eastern shore of Georgian Bay. Across strike, it is 400 km wide (Davidson 1984b). The main metamorphic and structural event of the Grenville Province occurred during the Grenvillian Orogeny, "a polyphase tectonic event ... that affected the southeastern Canadian Precambrian Shield, culminating between 1.15 and 1.0 Ga" (Davidson 1985, p 137).

Wynne-Edwards (1972) divided the Grenville Province into six subprovinces (Fig. 1.1). The Central Gneiss Belt, one of these subprovinces, is an area of mostly quartzofeldspathic gneisses (Davidson 1984b). Within the Central Gneiss Belt there are ductile shear zones which are the loci "of high strain concentration formed during ductile deformation deep in the crust along which large crustal blocks and slices have been displaced with respect to one another" (Davidson 1985, p 140). These ductile shear zones juxtaposed assemblages of different rock types during continental convergence and crustal thickening. Two of these assemblages, the Britt and the Parry Sound domains, lie within the study area. The Britt Domain (Fig. 1.2), an assemblage of amphibolite facies rocks, is subdivided into five distinct gneiss associations (Culshaw et al. 1988). These may represent terranes assembled in the mid-Proterozoic or earlier, or Grenville thrust sheets.

The Parry Sound Domain lies to the south of the Britt Domain. It is an assemblage of granulite facies rocks overthrust onto the Britt Domain, (Davidson 1986). Figure 1.2 shows the geology of the study area, including relevant portions of the Britt and Parry Sound domains.

The presence of assemblages equilibrated at 8 - 10 kb (Corrigan 1990, Ketchum 1991, pers comm) suggests that the present day surface was once at 24 - 30 km depth. As well, Rivers et al. (1989) believe that the Grenville Province was once comparable to large mountain belts of today, and as such it "presents an unrivaled opportunity to study orogenic processes at mid- to deep crustal levels" (Culshaw et al. 1991, p 3).

1.2 Historical Background

Mapping of the Grenville Province has taken place for more than a century with Logan (1847, 1863) and Wilson (1918, 1925) identifying some of the first elements. As a result of its complex nature and general lack of economic minerals, the Ontario segment of the Grenville Province has received less attention than other areas in this time (Davidson, 1986). Davidson and coworkers (1981, 1982, 1984, 1985, 1986) and Culshaw and coworkers (1983, 1988, 1989, 1990) carried out recent work in the Central Gneiss Belt of western Ontario. Ellsworth (1932) obtained the first radiometric date from the Grenville Province by using uraninite-bearing pegmatites from the Bancroft area (Easton 1986). Easton (1986) documented 1400 radiometric dates from the Grenville Province between 1932 and 1985. Methods used include K-Ar, Ar-Ar, Rb-Sr, Nd-Sm, and U-Pb.

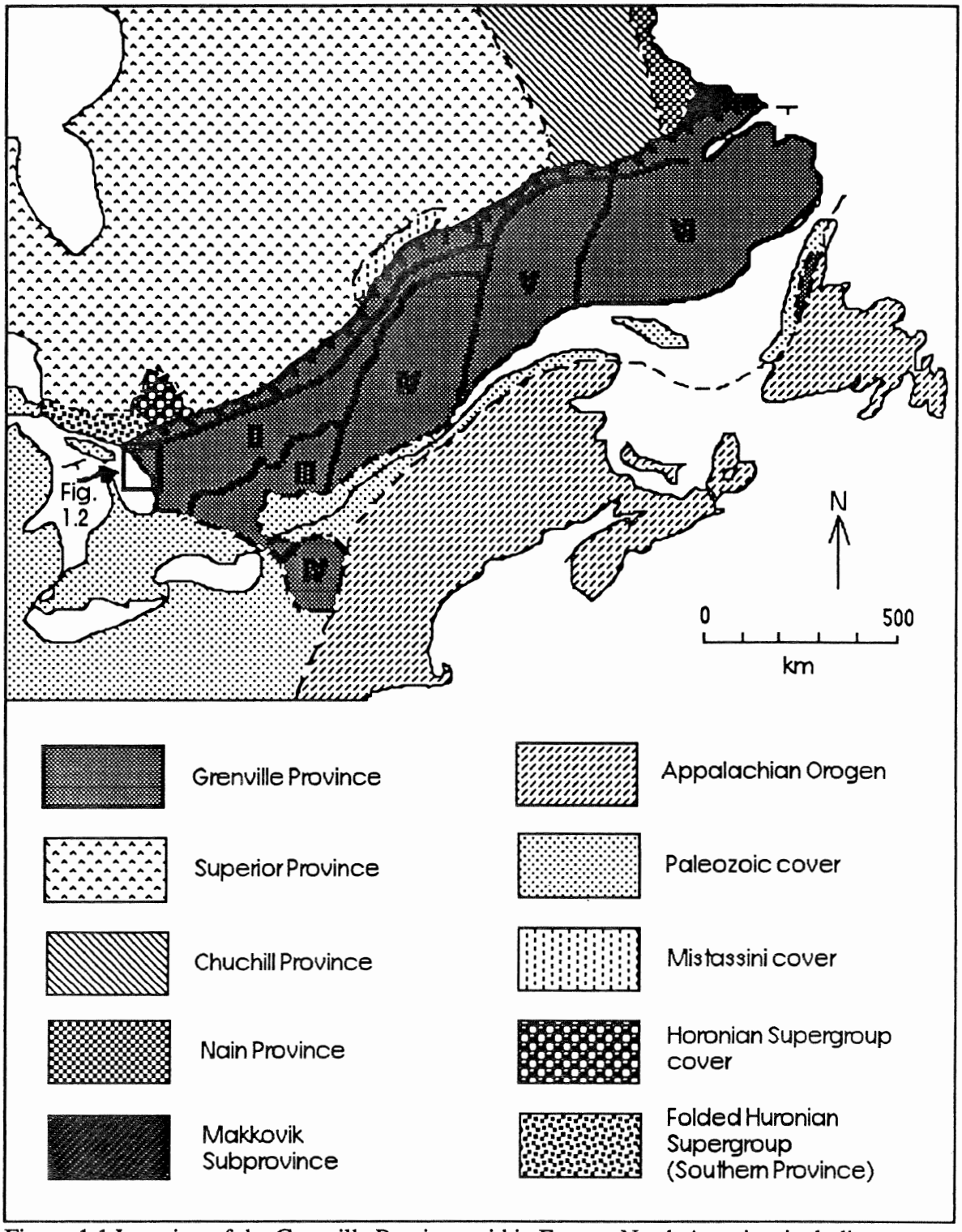

Figure 1.1 Location of the Grenville Province within Eastern North America, including major subdivisions (after Davidson 1984b). I: Grenville Front Tectonic Zone, II: Central Gneiss Belt, III: Central Metasedimentary Belt, IV: Central Granulite Terrane, V: Baie Comeau Segment, VI: Eastern Grenville Subprovince. Location of Figure 1.2 is shown.

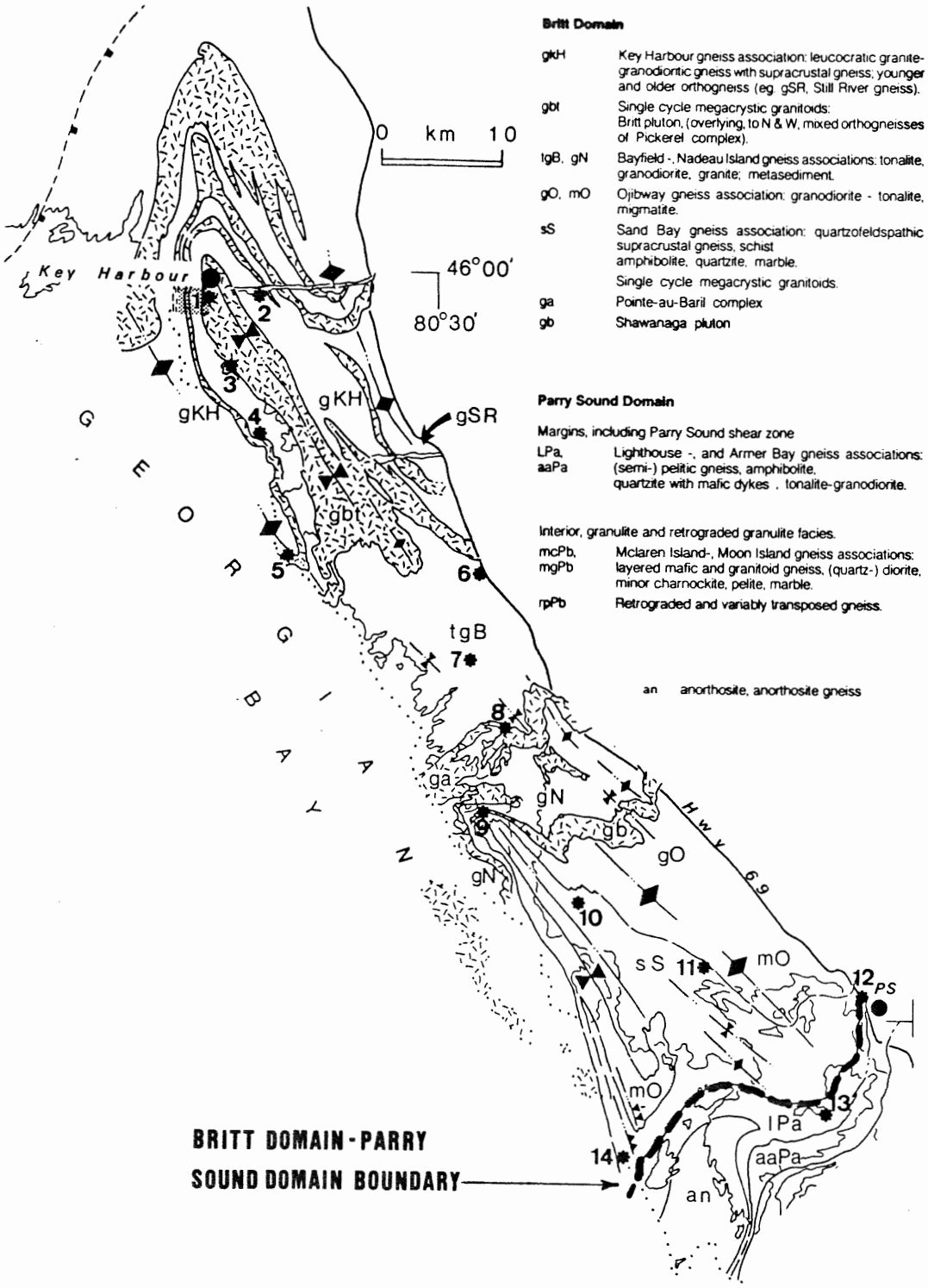

Figure 1.2 Geology of the study area, and sample locations (after Culshaw et al. 1988, 1989). PS: Parry Sound. ✷1: Sample #1. Refer to Appendices 1 and 2 for site and sample descriptions.

Within the Central Gneiss Belt, numerous radiometric studies have been carried out. Workers such as Corrigan et al. (1990), Davidson and Breemen (1988), and van Breemen et al. (1986) used these methods in an attempt determine the age of emplacement of plutonic rocks, metamorphism, and deformation. Others, such as Cosca et al. (1990), and Culshaw et al. (1991) used radiometric methods to investigate post-tectonic cooling and thermal histories.

In a study of post-tectonic cooling, Culshaw et al. (1991) carried out a $^{40}Ar/^{39}Ar$ study of the Britt Domain (Fig. 1.2) using amphibole, biotite, and K-feldspar from granitoid plutons of mid-Proterozoic age, and muscovite from paragneiss of the country rock. From north to south, muscovite ages decreased approximately 20 Ma. Since the samples passed through hornblende closure temperature at least 20 Ma after deformation ceased, Culshaw et al. (1991) considered the data to be a record of post-tectonic thermal history in the orogen.

Cosca et al. (1990) also did a $^{40}Ar/^{39}Ar$ study using muscovite, among other minerals, but farther south in the Central Gneiss Belt. Their most northerly sample, which is approximately on strike with the most southerly of Culshaw et al. (1991), is the oldest. This pattern of decreasing age with increasing distance from the Grenville Front Tectonic Zone led Culshaw et al. (1991) to suggest tentatively a decrease in cooling rate to the south.

1.3 Purpose, Direction, and Scope of Study

The motivation for this study is the need to investigate further the apparent decrease in age of muscovites across the orogen from the Grenville Front Tectonic Zone. If such a trend is present, it may have significant implications for

the post-tectonic thermal history of the orogen. To date, the apparent trend in ages is based on only four ages. Therefore, determination of more ages from the same area is required to substantiate a trend. Reexamination of the earlier data (Culshaw et al. 1991) helps to qualify the interpretation.

$^{40}Ar/^{39}Ar$ analysis of a suite of fourteen muscovite samples is the basis of this study. Samples came from the northern end of the Parry Sound Domain to the northern end of the Britt Domain (Fig. 1.2). Petrological description of the samples accompanies details of their processing and analysis.

An overview of radiometric dating provides necessary background information. The theory behind the actual techniques used in this study follows this, with attention paid to aspects such as closure temperature and argon loss. These are of importance to the interpretation of the data.

Interpretation and discussion lead to two uplift models. These are intended to help explain the history of this part of the Grenville Province.

Appendices elaborate on some of the details of this study. These include the petrographic, mathematical, and numerical background to much of the information summarized in the main body of this thesis.

Conclusions apply primarily to the study area. In future the model presented should be tested against similar data from other parts of the Grenville Province. From this, a better understanding of post-tectonic uplift and cooling in major orogenic belts may evolve.

CHAPTER 2: SAMPLES

2.1 Sampling

Culshaw and coworkers collected all samples during the summers of 1987 - 1990, inclusive, as part of the Georgian Bay Geological Transect. Appendix 1 gives the sample location and code name assigned by Culshaw for each sample, to facilitate comparison with related studies. For this study, the samples are numbered 1 through 14, north to south, respectively.

Samples 1, 3, 9, and 14 come from Culshaw et al. (1991). All others were prepared and analysed specifically for this study. Because the method of analysis used was the same in each case, the two data sets have been combined for interpretation.

2.2 Petrology

Culshaw (1991, pers comm) believes that all samples are metasedimentary in nature. Petrographic examination and interpretation supports this idea in most cases.

Appendix 2 details the results of hand specimen and thin section analysis of each sample. Photomicrographs accompany the descriptions. Muscovite received particular attention, because of its importance in the radiometric analysis.

Tables 2.1 and 2.2 summarize the petrologic results. Sample mineralogy and muscovite characteristics such as form, texture, alteration, deformation, and orientation help identify similarities and differences among samples. The quality of these characteristics may help explain radiometric ages that do not appear appropriate. For example, mineral spectra with poor or no plateaux (discussed in Chapter 4) may

correlate with muscovite grains with unique, or deformed textures.

In general, most samples contain significant amounts of feldspar, and commonly quartz. Biotite is almost always present. The muscovite grains usually fit one of two general descriptions. Some are in the form of short (length:width < 5:1), tabular, euhedral or subhedral, decussate grains. Others may be longer (length:width > 5:1), euhedral, subhedral, or anhedral, bent grains.

#	Rock Type	Mineralogy
1	quartzofeldspathic pelitic gneiss	Ms Qtz O Bt Crn
2	quartzofeldspathic pelitic gneiss	Ms Qtz Afs Kfs Crn
3	quartzofeldspathic gneiss	Ms Afs ± Bt Qtz Chl
4	quartzofeldspathic gneiss	Kfs Ms O ± Ky Qtz
5	quartzofeldspathic gneiss	Kfs Afs Bt Ms ± Qtz
6	quartzofeldspathic migmatitic gneiss	Qtz Afs Bt Ms Kfs
7	quartzofeldspathic pelitic gneiss	Ms Kfs Afs Bt Gr ± Qtz
8	schist	Ms Kfs Bt O
9	quartzofeldspathic gneiss	Afs Qtz Ms Bt ± Ky Crn
10	quartzofeldspathic gneiss	Qtz Afs Ms Bt
11	quartzofeldspathic gneiss	Qtz Ms Afs Bt ± Hem
12	schist	Ms Bt Afs Qtz Grt
13	schist	Ms Afs Qtz Bt Grt ± Chl St O
14	quartzofeldspathic gneiss	Qtz Bt Kfs Afs Ms

Table 2.1 General petrology of samples. Refer to Appendix 2 for complete details. Mineral abbreviations (after Kretz 1983): Afs: alkali feldspars, Bt: biotite, Chl: chlorite, Crn: corundum, Grt: garnet, Hem: hematite, Ky: kyanite, Ms: muscovite, O: opaques, Kfs: K-feldspars, Qtz: quartz, St: staurolite.. # refers to sample number.

	Samples						
Characteristics	1	2	3	4	5	6	7
apparent length:width	2:1	2:1	3:1	5:1	4:1	2:1	5:1
extinction	ub	ub	b	ub	b	b	b
straight	+	+	+	±	+	+	+
inclusions	+	–	–	–	–	–	–
micrographic	+	+	+	+	–	+	–
altered	+	–	–	–	–	–	–
grain boundaries	sa	sa±d	esa±d	sa	esa	sa	esd
clustered	–	–	–	–	–	–	–

	8	9	10	11	12	13	14
apparent length:width	3:1	3:1	2:1	4:1	10:1	10:1	15:1
extinction	b	b	±b	bu	bu	bu	b
straight	+	+	+	+	–	–	+
inclusions	–	–	–	+	+	–	–
micrographic	–	–	+	+	+	+	+
altered	–	–	–	–	–	–	–
grain boundaries	esd	sa	esad	esd	sa	esd	esd
clustered	+	–	–	–	+	–	–

Table 2.2 Comparison of muscovite grain characteristics. "Straight" grains are no bent or physically deformed.+ indicates presence of characteristic in sample, - indicates absence, and ± indicates minor presence. u: undulose, b: bird's eye, e: euhedral, s: subhedral, a: anhedral, d: decussate. Appendix 2 contains more complete descriptions, including photomicrographs.

CHAPTER 3: LABORATORY PROCEDURES

3.1 Sample Preparation

Whole-rock samples containing visible muscovite were crushed, sieved, washed, dried, and then sieved again to obtain 125 μm - 210 μm fractions. The fraction was poured onto a sheet of paper and the paper was tilted, according to the paper panning method. Blocky minerals, such as quartz and feldspars, rolled off the paper while the platy micas remained. A Frantz magnetic separator separated the muscovites from the biotites by their magnetic susceptibilities to obtain fractions greater than 99% pure.

The muscovites were irradiated with fast neutrons in the McMaster University nuclear reactor for ten hours. Before mass spectrometric analysis, the samples remained undisturbed for two months.

3.2 Sample Analysis

Muscovite samples were analysed by two mass spectrometers. An A.E.I. MS-10 mass spectrometer analysed samples 1, 3, 5, 6, 7, 8, 9, 11, and 14. A VG3600 mass spectrometer analysed samples 2, 4, 10, 12, and 13. Figure 3.1 is a generalized diagram of a mass spectrometer system similar to the ones used in this study.

For each sample, an aliquot of irradiated muscovite was placed in an extraction furnace. The sample was heated in 11 - 13 steps from approximately 300°C to 1150°C to release trapped argon (known as outgassing). Each step represented an increase of 30 C° to 50 C° and lasted for approximately one hour.

After heating, the gas was collected in a charcoal finger held at -196°C by liquid nitrogen. A titanium "getter" removed impurities from the gas.

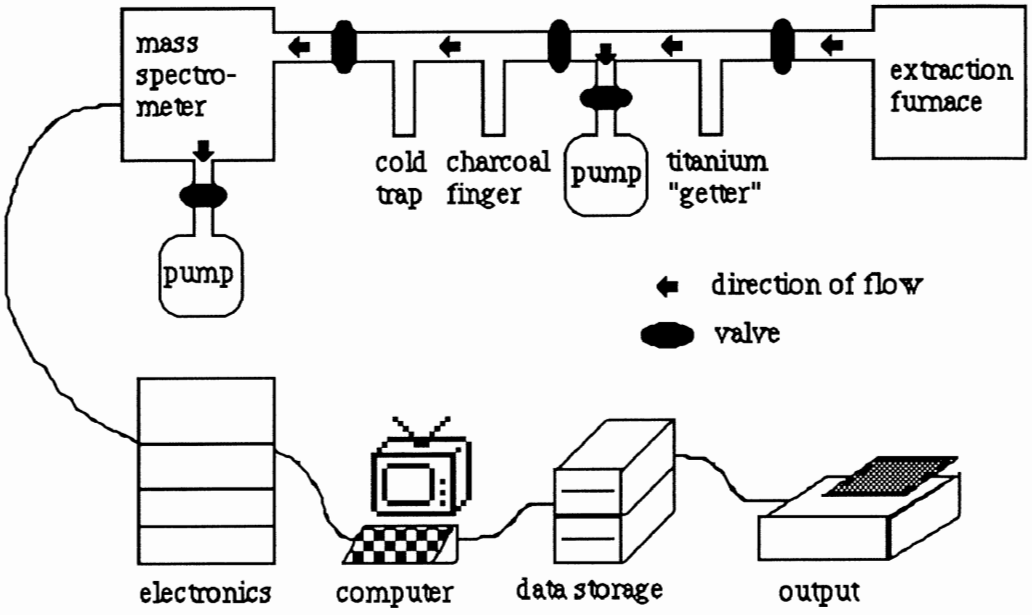

Figure 3.1 Generalized mass spectrometer system.

Once cleaned, the argon gas was admitted to the mass spectrometer. A liquid nitrogen cold trap removed any remaining impurities as the gas entered the mass spectrometer. The mass spectrometer analysed the gas for ^{36}Ar, ^{37}Ar, ^{39}Ar, and ^{40}Ar. A computer acquired the data, corrected for atmospheric and background argon, and calculated an age based on the amount of ^{39}Ar and radiogenic ^{40}Ar present.

After each heating step, the mass spectrometer was pumped free of the gas and the next step started. After completion of all steps, the computer produced a plot of apparent age versus cumulative $\%^{39}Ar$ released for all steps.

Chapter 4 and Appendix 3 describe the theory behind $^{40}Ar/^{39}Ar$ dating and how actual ages are calculated. The results are presented in Chapter 5 and Appendices 4 and 5.

CHAPTER 4: RADIOMETRIC DATING

4.1 Introduction

Some atoms spontaneously decay from their parent isotopes to daughter isotopes (Skinner and Porter 1987), i.e. the atoms give up parts of their nuclei to become lighter and more stable. This is radioactive decay.

Although the process is random, radioactive decay is statistically predictable for large numbers of atoms. The rate of decay of a parent isotope is proportional to the number of atoms present in the sample (Petrucci 1985). As well, each radioactive element has its own characteristic rate of decay. Many of these have been determined experimentally and are expressed as decay constants (Sharma 1987).

Another useful term is the half life. According to Skinner and Porter (1987, p 184), the half life is "the time required to reduce the number of parent atoms by one half." According to Sharma (1987), the half life, $t_{1/2}$, may be related to the decay constant, λ, by

$$t_{1/2} = (\ln 2) / \lambda \qquad (4.1)$$

The rate of decay of a radioactive element is not affected by geologic processes. Therefore, for rocks which contain minerals with radioactive elements, absolute age determinations may be made. The process, known as radiometric dating, involves the measurement of parent and daughter isotopes present.

Once isotopic measurements have been made, the following equation may be used to calculate the age of the sample:

$$t = (1/\lambda) \ln (1 + D/N) \quad (4.2)$$

where t is the age of the sample (in years), λ is the decay constant (in years^{-1}), D is the daughter isotopic count, and N is the parent isotopic count. This is the basic equation of geochronology (McDougall and Harrison 1988). Appendix 3 explains the derivation and use of this equation more fully.

Easton (1986, p 128) presents some assumptions that must be made when calculating ages from radiometric methods. These are:
"the decay constant is known and is constant";
"there is no gain or loss of parent or daughter isotopes other than by radioactive decay"; and
"all samples were initially isotopically homogeneous".
If any of these assumptions are not met, the calculated age will not be correct.

4.1.1 $^{40}K/^{40}Ar$ Dating

Potassium, a common element in the crust, has a radioactive isotope, ^{40}K, which decays to two daughter products, ^{40}Ar and ^{40}Ca. $^{40}K/^{40}Ar$ dating is a common radiometric technique (Sharma 1986). Table 4.1 shows the decay scheme of potassium, and other pertinent data.

According to Faure (1986), the accumulation of radiogenic argon (Ar^*) may be expressed as

$$^{40}Ar^* = (\lambda_\kappa/\lambda)\ ^{40}K\ (e^{\lambda t} - 1) \quad (4.3)$$

where $\lambda = \lambda_\kappa + \lambda_\beta$ (see Table 4.1). This is the K-Ar equation.

It may be rearranged to solve for t:

$$t = \frac{1}{\lambda} \ln \left[\frac{^{40}Ar^*}{^{40}K} \left(\frac{\lambda}{\lambda_\kappa} \right) + 1 \right] \qquad (4.4)$$

Parent Isotope:	^{40}K	
% of Natural Element:	0.001167	
Half Life (years):	$1.25 * 10^9$	
Decay Mechanism:	11% κ-electron capture:	89% β emission:
Stable Daughter:	^{40}Ar	^{40}Ca
Decay Constant (yrs^{-1}):	(λ_κ) $0.581 * 10^{-10}$	(λ_β) $4.962 * 10^{-10}$

Table 4.1 Decay scheme of Potassium (after Sharma 1987). Refer to Sharma (1987) for more detailed explanation of characteristics.

The measurement of ^{40}Ar and ^{40}K may be made by mass spectrometry, and wet chemistry, respectively. Because some of the ^{40}Ar measured may be atmospheric, a correction must be made with the help of ^{36}Ar which is non-radiogenic. The ratio of $^{40}Ar/^{36}Ar$ in the atmosphere is well known, so by measuring the amount of ^{36}Ar present in the sample, the amount of atmospheric ^{40}Ar may be calculated. This amount may then be subtracted from the total ^{40}Ar. The corrected ^{40}Ar value may then be used in the age calculation of equation 4.4 (Sharma 1986).

Because argon may diffuse from the host mineral at temperatures as low as 300°C, $^{40}K/^{40}Ar$ geochronometers may be reset during periods of metamorphism. In light of this phenomenon, the $^{40}Ar/^{39}Ar$ dating method may be used to provide a better thermal history (Reynolds 1991, pers comm).

4.1.2 $^{40}Ar/^{39}Ar$ Dating

$^{40}Ar/^{39}Ar$ dating is a variation of $^{40}K/^{40}Ar$ dating. It involves the irradiation of a mineral sample by fast neutrons in a nuclear reactor. This converts a portion of the ^{39}K atoms to ^{39}Ar, which is considered to be stable during the period of analysis. One of the advantages of this method is that both isotopes of argon may be measured by mass spectrometry at the same time. Because the amount of ^{39}Ar produced is proportional to the amount of ^{39}K present in the original sample, and the amount of ^{39}K is proportional to the amount of ^{40}K present, the amount of ^{40}K may be calculated from the amount of ^{39}Ar measured. The age of the sample may then be calculated by using the equation

$$t = 1/\lambda \ln ((^{40}Ar^{*}/^{39}Ar)\ J + 1) \qquad (4.5)$$

Appendix 3 contains the derivation of this equation, as well as the calculation of its error.

Another advantage of the $^{40}Ar/^{39}Ar$ method is the incremental heating technique. Incremental heating allows a sample to be outgassed of argon incrementally over a series of temperature increases. If the isotopic system were closed since the time of formation, then the gas produced by each step should give the same age when analysed. As was noted previously, radiogenic argon may be lost because of diffusion at temperatures well below that of the event under investigation. The incremental heating technique allows dates to be calculated based on parts of the mineral which may have lost different amounts of radiogenic argon since formation. This provides an opportunity to calculate an age based on the part of the mineral which lost the least argon. Without this

technique, only an average for the whole sample would be available (Faure 1986).

4.2 Closure Temperatures

The exact meaning of dates obtained from radiometric analyses requires further explanation. According to the theory of radiometric methods examined in Section 4.1, the age of a mineral is the time since a radioactive isotope in a mineral began to decay to a daughter isotope. This age also requires that none of the daughter product escapes after formation. A better definition of this age is the time since a mobile radioactive isotope became immobile within the crystal lattice of the mineral. Mobility refers to the ability of the isotopes (both parent and daughter) to diffuse from their locations within the crystal lattice (Dodson 1973).

The traditional view of mobility is that it ends at the point of crystallization or recrystallization. In the late 1960s and early 1970s new evidence suggested that mobility continued, in some cases, well below crystallization and recrystallization temperatures. The radiometric age of a mineral is, therefore, the time since the mineral cooled through this "closure temperature" (also known as blocking temperature) (Dodson 1973, p 259).

Figure 4.1 gives a graphic definition of closure temperature. At high temperatures the rate of diffusion (of the radiogenic isotope) is greater than the rate of accumulation, so that no radiogenic isotope accumulates. As the temperature decreases, the rate of accumulation increases until essentially all of the radiogenic isotope produced is retained in the crystal lattice. Extrapolation of the low temperature part of the accumulation line to zero provides

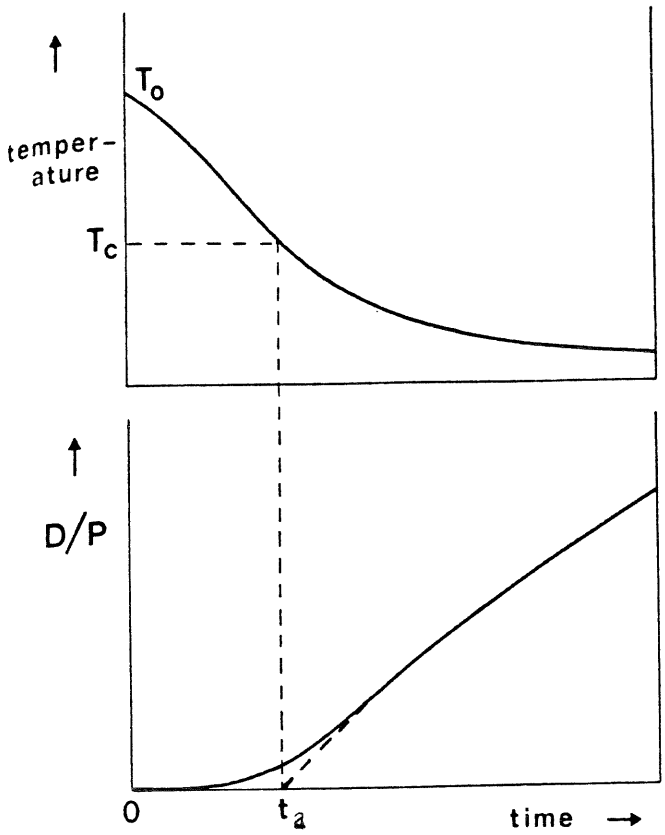

Figure 4.1 Definition of closure temperature (after Dodson 1973). T_0 is the initial temperature, t_a is the apparent age, T_c is the closure temperature, and D/P is the ratio of accumulated daughter to residual parent isotopes. See text for further explanation.

the apparent age of the sample on the time axis. This point may then be projected vertically to the temperature curve to determine the closure temperature of the mineral (Dodson 1973).

4.2.1 Muscovite Closure Temperature

Laboratory attempts to determine the closure temperature of muscovite, the mineral radiometrically analysed in this study, have not been entirely successful (McDougall and Harrison 1988). Snee et al. (1988) did a literature search of muscovite closure temperature and arrived at the value of 320° ± 40° C. This is the value used in this study.

CHAPTER 5: RESULTS

5.1 Age Interpretations

Appendix 4 contains analysis summaries for all samples. Appendix 5 contains plots of calculated ages against % ^{39}Ar, known as mineral age spectra.

From these spectra, and the corresponding analysis summaries, interpretation of ages is possible. The simplest way is to calculate a weighted average of the results of all fractions of the gas. This is known as the total gas age. At the bottom of each summary sheet is a total gas age.

Examination of the argon release spectra reveals that they are not flat. During incremental heating, the earliest gas released comes from the outer edges of the mineral grains. These parts of the grains are the most likely to have lost argon since passing through the closure temperature. Therefore, this gas indicates a younger age. As temperature increases, gas is released from regions deeper within the grains. Calculated ages become greater until they reach a maximum. In terms of the spectrum, this maximum age may appear as a plateau (Faure 1986). This plateau age is more representative of the time of cooling through the closure temperature.

Fleck et al. (1977, p 19) define a plateau as "that part of an age-spectrum diagram composed of contiguous gas fractions that together represent more than 50% of the total ^{39}Ar released from the sample and for which no difference in age can be detected between any two fractions at the 95% level of confidence." The latter requirement may be tested with the "critical value" test. This critical value may be calculated as

$$C.V. = 1.960\ (\sigma_1^2 + \sigma_2^2)^{1/2} \qquad (5.1)$$

where σ_1^2 and σ_2^2 are the standard deviations of the ages. No two ages may differ by more than the critical value.

In most cases, definition of a plateau age was possible. However, in the case of sample 2, the data failed the definition of Fleck et al. (1977) in a minor way. Step 13 was omitted because it was anomalously low. This age is designated a "modified plateau age."

In two cases, no plateau existed. For these samples, weighted averages of all but the earliest steps were used to calculate ages. These ages are designated "modified total gas ages."

Sample	Age (Ma)	Comments
1	924 ± 3	plateau age
2	906 ± 4	modified plateau age
3	922 ± 3	plateau age
4	907 ± 4	plateau age
5	904 ± 4	plateau age
6	899 ± 4	plateau age
7	893 ± 4	plateau age
8	898 ± 4	modified total gas age
9	904 ± 3	plateau age
10	892 ± 4	plateau age
11	898 ± 4	plateau age
12	884 ± 2	plateau age
13	892 ± 2	modified total gas age
14	905 ± 3	plateau age

Table 5.1 Apparent ages of samples and distances from sample 1.Techniques of determining ages are described in the text.

Table 5.1 lists the calculated ages for all samples. Appendix 6 provides an example of plateau age calculation, as well as explanations of particular age calculations.

5.2 Age Adjustments

The samples of Culshaw et al. (1991) (1, 3, 9, and 14; referred to as "the earlier set") appear to be significantly higher in age than closely located ones processed for this study. Reexamination of the data for the earlier set revealed doubt over the accuracy of the J values (discussed in Appendix 3) used in calculating the original ages. As the same J value applied to all four samples, the ages obtained were all satisfactory relative to each other. Their absolute values were less certain, and awaited further samples from the same area to assist in better definition (Reynolds pers comm 1991).

The four ages from the earlier set have been reevaluated in accordance with the new ages, for which the J value was better determined (Reynolds pers comm 1991). Because both subsets span the same geographic area, their average ages should be the same. Calculation of these averages revealed the earlier set to be, on average, 15.5 Ma older than the new set. This value has been subtracted from each age from the earlier set. Table 5.2 lists these adjusted ages. Appendix 6 more fully explains the procedure of adjustment.

5.3 Final Ages, Errors, and Reliability

Table 5.2 ranks ages in terms of reliability. Increasing number represents decreasing reliability. Those ranked 1 are plateau ages, those ranked 2 are modified plateau ages, and those ranked 3 are modified total gas ages. Sample 7 received

a rank of 4 because its spectrum displays a pattern that suggests the sample lost a significant portion of its ^{40}Ar after cooling through its closure temperature. This is also suggested by the anomalously low calculated age. For these reasons, this sample has been omitted from further consideration in this study.

The error of each sample is based on the error of its J value. Appendix 6 explains the calculation of these errors, with an example.

Sample	Age (Ma)	Reliability	Comments
1	907 ± 3	1	recalculated
2	906 ± 4	2	
3	906 ± 3	1	recalculated
4	908 ± 4	1	
5	904 ± 4	1	
6	899 ± 4	1	
7	893 ± 4	4	displays argon loss pattern
8	896 ± 4	3	
9	887 ± 3	1	recalculated
10	892 ± 4	1	
11	901 ± 4	1	
12	884 ± 2	1	
13	892 ± 2	3	
14	888 ± 3	1	recalculated

Table 5.2 Adjusted ages of samples, including errors, and reliability.Techniques of adjusting ages and error calculation are described in the text. Reliability is based on method of calculation.

CHAPTER 6: INTERPRETATION

6.1 Age Versus Distance

Figure 6.1 shows the sample locations projected to a common line perpendicular to the strike of the orogen. This line (146°) is parallel to the hinges of major folds, stretching lineations, and direction of orogenic transport. The reason for using this arrangement is to investigate the relation of the data to the cross-sectional geometry of the orogen. Distances of the samples are all relative to a point on the line just north of sample 1 (Key Harbour). Table 6.1 lists these distances and the ages of the samples.

Sample:	Distance From Key Harbour (km):	Age (Ma):
1	1.0	907 ± 3
2	3.2	906 ± 4
3	5.9	906 ± 3
4	13.0	908 ± 4
5	22.8	904 ± 4
6	32.8	899 ± 4
8	45.0	896 ± 4
9	49.8	887 ± 3
10	60.7	892 ± 4
11	70.7	901 ± 4
12	79.8	884 ± 2
13	86.5	892 ± 2
14	80.4	888 ± 3

Table 6.1 Adjusted ages of samples and distances from Key Harbour.

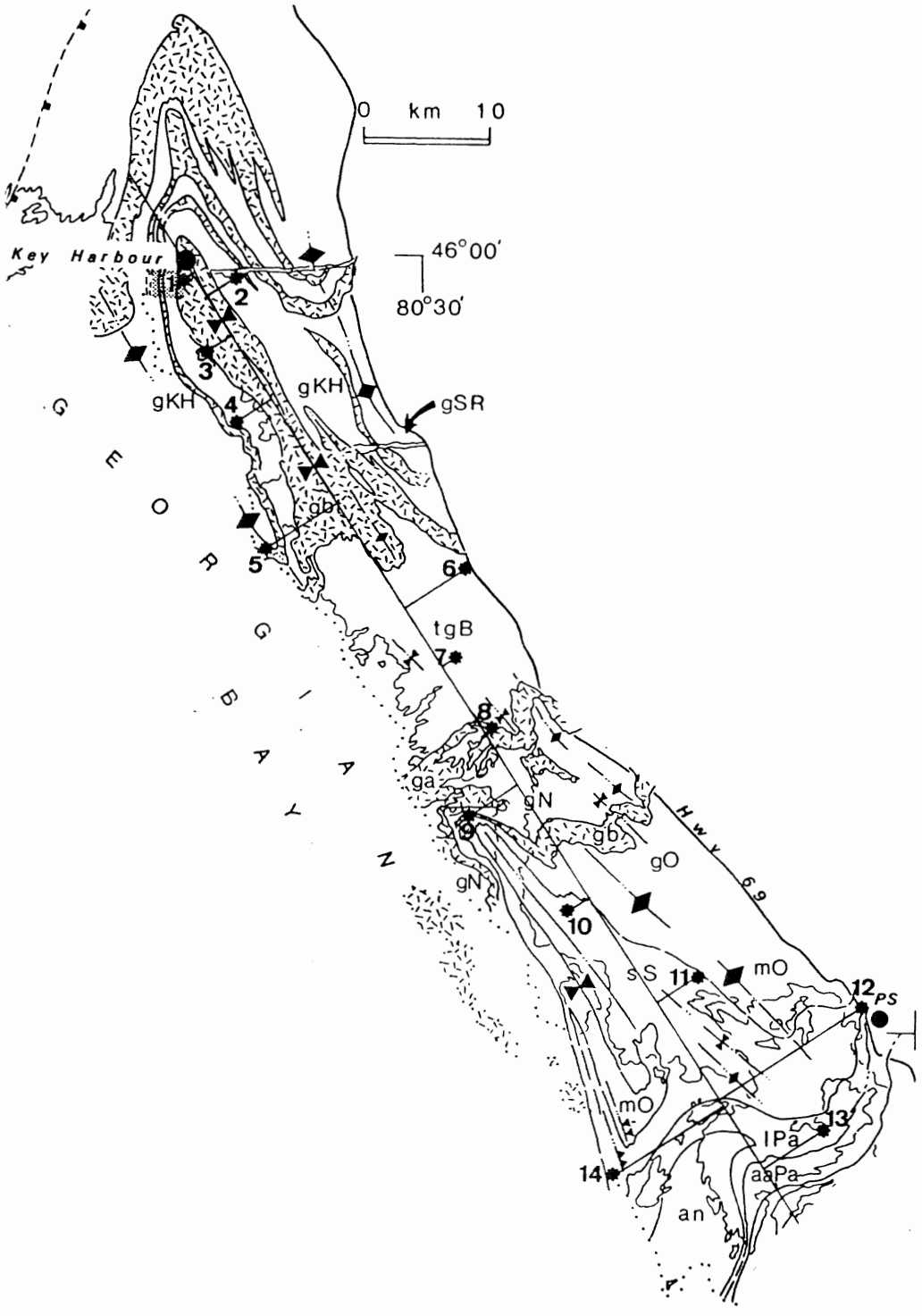

Figure 6.1 Projection of sample locations to a common line.

Figure 6.2 is a plot of apparent age versus distance. The equation of the linear regression line through the data is

$$y = -0.22563x + 907.28 \qquad (6.1)$$

where y is the age of the sample, in Ma, and x is the distance of the sample from Key Harbour, in km. The coefficient of determination (R^2) for this relationship is 0.712. An R^2 value this close to 1 argues favourably for a linear relationship among the data.

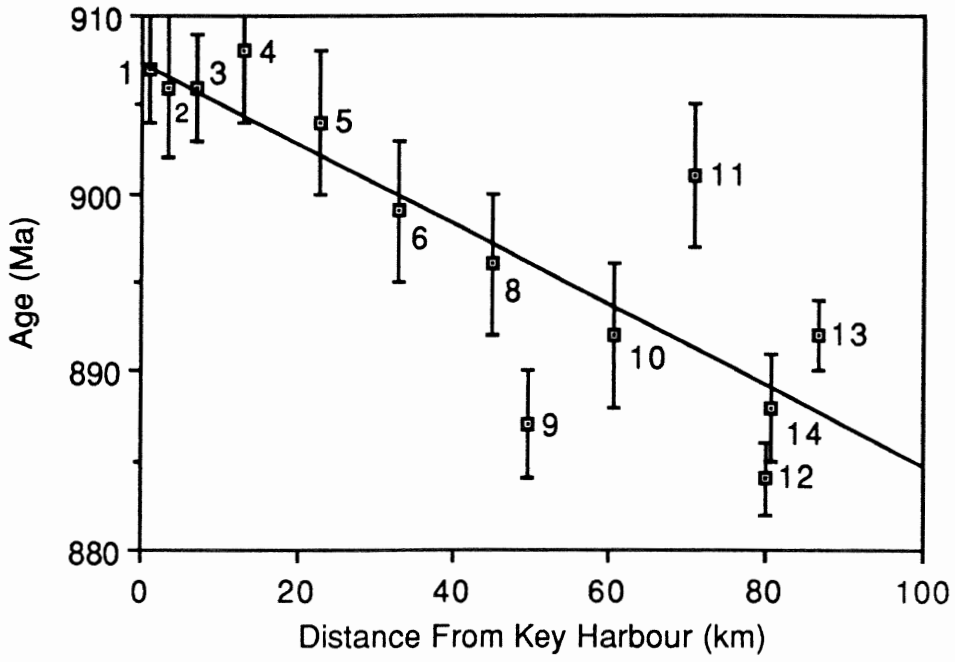

Figure 6.2 Plot of apparent age versus distance from Key Harbour. Numbers refer to samples.

6.2 Discussion

Examination of Figure 6.2 reveals two features of the trend. Ages in the north conform to the line much better than those in the south. Samples 9, 11, 12, and 13 are so far from their predicted values that even their error bars do not lie on the line. Most of these samples come from the vicinity of the Britt Domain - Parry Sound Domain boundary. Although the duplexing event which created this boundary may have altered local isotherms, Culshaw (1991, pers comm) believes this event was too early to affect the times of closure of the muscovite in these samples.

Petrographic examination (Chapter 2, Appendix 2) offers possible explanations for some of these deviations. Muscovite in sample 11 contains hematite inclusions. If the presence of hematite increases the argon retentivity of muscovite, then the calculated age of sample 11 may be unrealistically old.

The muscovites of sample 13 are crenulated, possibly because of a later deformational event. If this event caused new argon to become trapped in the muscovite, then the sample would appear anomalously old.

6.3 Models

The ages of these samples decrease 0.23 Ma / km, north to south. Because the samples passed through the closure temperature at different times, two possible explanations arise:

(1) The samples were at different depths in the crust in the past, and the geothermal gradient was constant across the orogen.

(2) The samples were always at the same depth, but the geothermal gradient varied across the orogen.

The following models explore these possibilities.

6.3.1 Variable Uplift

This model assumes that the closure temperature of muscovite represents a common depth in the crust. For these samples to have passed through a common depth point at different times requires that they experienced different uplift rates.

One way of exploring the effect of variable uplift rates on the data is mathematical modelling. 1DT is a program which allows modelling of one-dimensional geothermal histories on IBM PC computers (Haugerud 1989). Culshaw et al. (1991) used this program to produce a one-dimensional thermal model of the Britt Domain (Fig. 6.3). Age and closure temperature data from several sets of different minerals defined an uplift history consisting of five stages of decelerating uplift. While this model is not unique, it is plausible (Culshaw 1991, pers comm). Appendix 7 discusses the assumptions and parameters of this model.

Figure 6.4 illustrates the use of 1DT to determine different uplift rates for each end of the transect. The boxes represent the ranges of ages and possible closure temperatures of hornblende (Culshaw et al. 1991) and muscovite (this study). The hornblende box is at the start of the third stage of uplift, while the muscovite box is at the end of this stage. Adjustment of the uplift rate of stage 3 resulted in the temperature-time path passing through the muscovite box at different points. Table 6.2 is a summary of calculated uplift rates for each end of the transect (908 ± 4

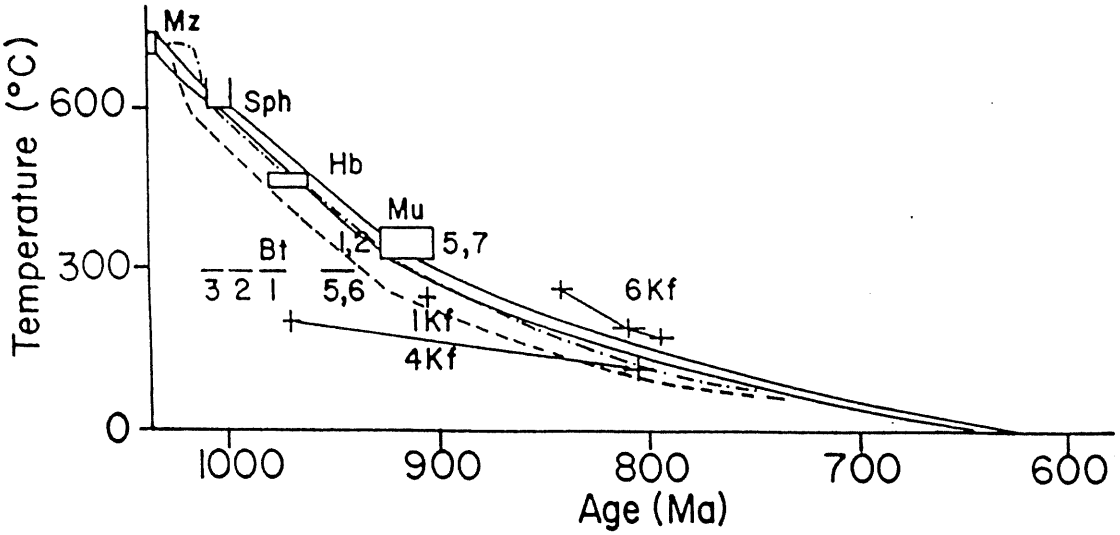

Figure 6.3 One-dimensional thermal model of the Britt Domain (after Culshaw et al. 1991). Bt: biotite, Hb: hornblende, Kf: K-feldspar, Mu: muscovite, Mz: monazite, Sph: titanite. Numbers refer to locations of Culshaw et al. (1991). 1, 2, 4, 5, and 7 are the same as locations 1, 3, 5, 9, and 14 of this study. 3 is midway between locations 4 and 5 of this study, and 6 is 5 km south of sample 10 of this study. Appendix 7 describes the model parameters.

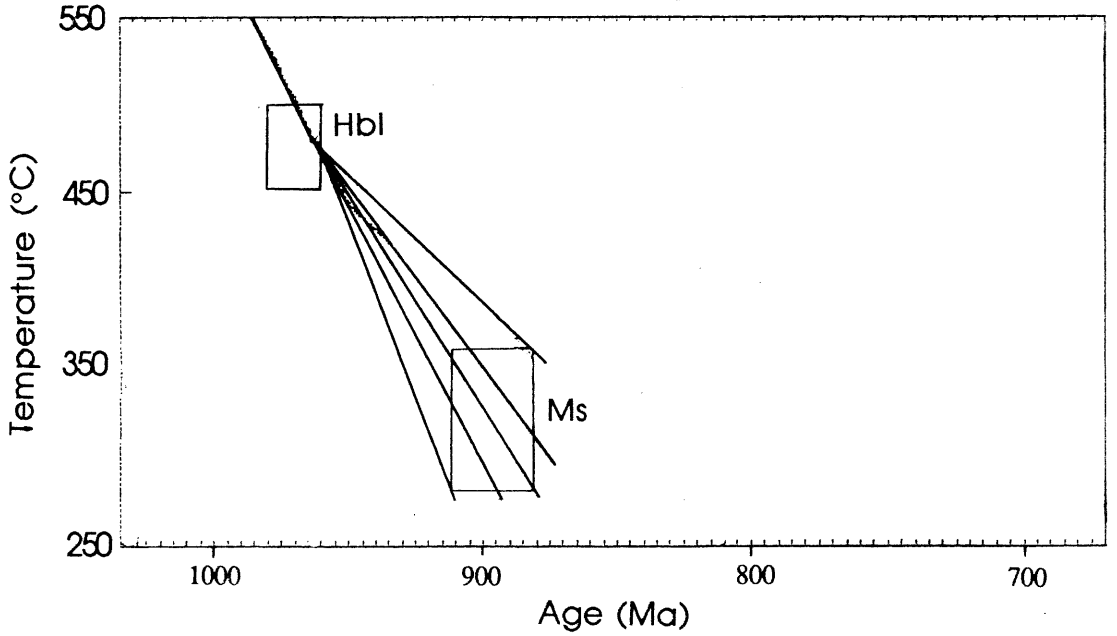

Figure 6.4 Method of determining effect of different uplift rates on samples of different ages and closure temperatures. Adjustment of stage 3 uplift rate causes temperature-time path to cross muscovite (Ms) box at different points. Hornblende (Hbl) end of stage remains fixed.

Ma and 884 ±2 Ma) at three different closure temperatures (360°, 320°, and 280°).

	uplift rate (mm / year)		% decrease
temperature	north end	south end	(N to S)
360° C	0.06	0.03	50
320° C	0.10	0.05	50
280° C	0.14	0.07	50

Table 6.2 Calculated uplift rates for stage 3 of model. See Appendix 7 for complete details.

Altering the uplift rate to fit various ages and temperatures showed that the data could be satisfied by a 50% decrease in uplift rate from the north end of the transect to the south, over a minimum of 80 Ma. More generally, it demonstrated that a decrease in uplift rates into the orogen is a possible cause of the trend in ages.

6.3.2 Variable Geothermal Gradients

This model assumes that the rate of uplift is constant across the orogen, but the geothermal gradient varies laterally.

Gaudemer et al. (1988) proposed that isotherms are offset vertically in a continental collision zone. In wide orogens, the interior of the continent heats up as a result of radioactive decay and lack of erosion. The frontal thrust zone, however, tends to be cooler than the interior of the orogen because of subduction of the lithospheric mantle along the Moho.

Figure 6.5 illustrates the model of Gaudemer et al. (1988). In Figure 6.5 (a), the shortening rate is held

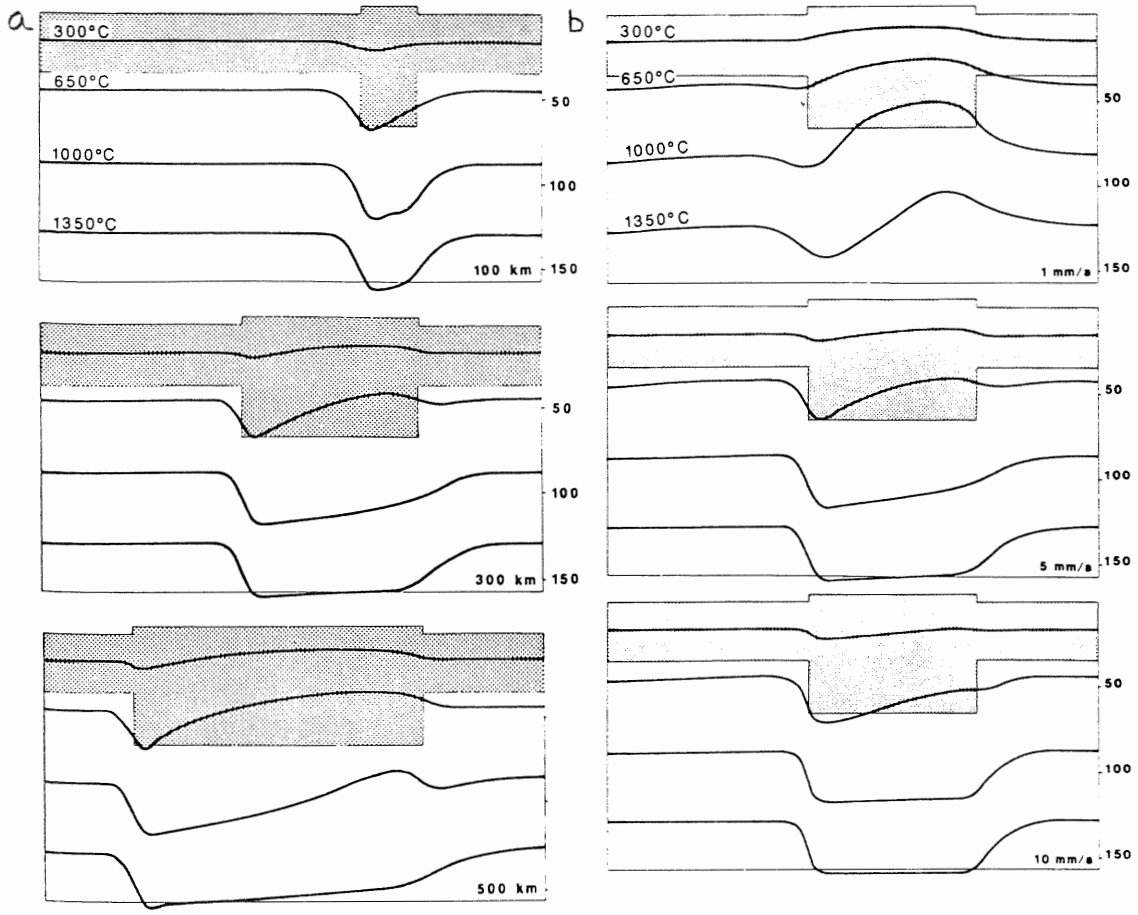

Figure 6.5 "Influence of belt width and shortening on the thermal structure of a collision belt. Selected isotherms are shown at the end of collision, prior to erosion." a: "Influence of belt width for a given shortening rate (5 mm / a). Parameters used in the calculations are $K_c = 2.5$ W / m K, $Q_c = 7 * 10^{-7}$ W / m ^{3}". b: "Influence of shortening rate for a given width (300 km)." Thermal parameters of b are the same as in a (after Gaudemer et al. 1988, p 53).

constant and the width of the orogen is varied. Depression of isotherms occurs below narrow orogens. For wider orogens, isotherms dip downward at the frontal thrust zone, but rise in the interior. Figure 6.5 (b), holds the orogenic belt width constant while varying the rate of shortening. All three rates result in depressed isotherms at the frontal thrust zone, but only the lower rates produce higher isotherms in the orogenic interior.

Isotherm depression near the frontal thrust zone is a common feature of all the models. Minerals of the same species at a common depth, but located at different distances from this front and rising at the same rate, would pass through their closure temperature at different times. They would reach the surface simultaneously, yet display different ages.

The program 1DT also has potential to investigate this model. Estimation of two different geothermal gradients based on the model of Gaudemer et al. (1989) led to two 1DT models. The first, calculated close to the frontal thrust zone, has a shallower gradient. The second, calculated farther from the frontal thrust zone, has a steeper gradient. Appendix 7 contains the details of these calculations.

The two new geothermal gradients replaced the original one, while all other variables remained as in the original model. Figure 6.6 shows the results. The shallower gradient caused the temperature-time path to pass through the muscovite closure temperature box slightly earlier than the temperature-time path influenced by the steeper gradient. These results show that a variable geothermal gradient can affect the times at which same-depth samples pass through a given temperature.

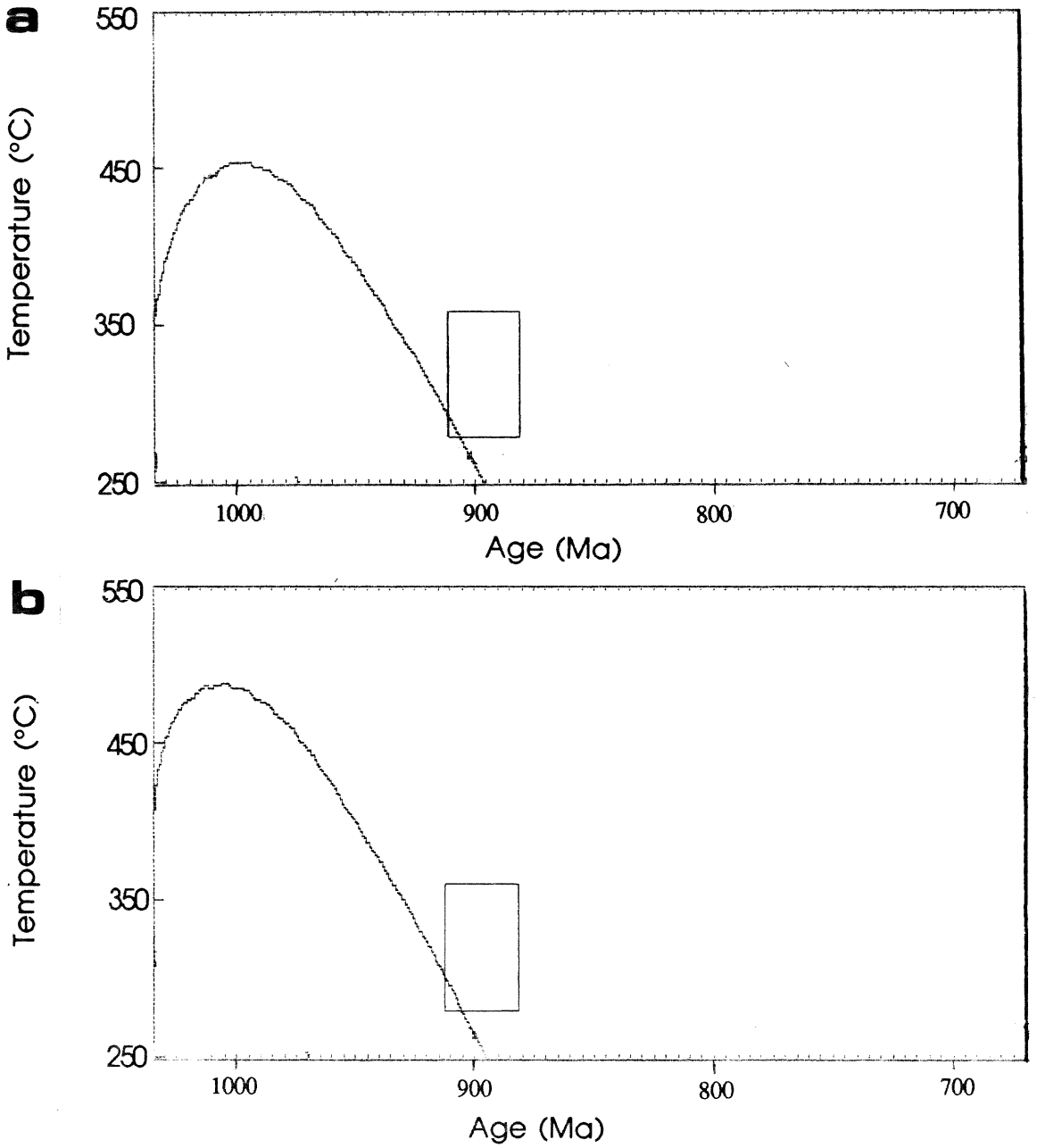

Figure 6.6 Temperature-time paths for two different geothermal gradients, starting at 30 km depth and. Figure 6.6 a is a shallower gradient which brings samples in contact with muscovite closure temperature slightly earlier than the steeper gradient of Figure 6.6 b. Appendix 6 explains the derivation of the two geothermal gradients.

6.3.3 Discussion

A possible explanation for variable uplift rates across the orogen is differential erosion. According to Gaudemer et al. (1988), erosion affects the outer edges of orogenic belts more than the interiors. The northern end of the transect is closer to the outer edge of the orogenic belt. It is, therefore, possible that this end of the transect experienced greater erosion which led to greater uplift.

The model of Culshaw et al. (1991) suggests that the samples were at roughly the same depth and followed the same uplift path at least until the hornblendes passed through their closure temperature. After this, the northern end of the transect experienced more rapid uplift at least until the samples passed through muscovite closure temperature. K-feldspar data indicate that the two ends of the transect continued along different uplift paths. Culshaw et al. (1991) assumed that the present day surface was attained sometime in the Late Proterozoic / Early Cambrian. Unless relative uplift rates were reversed, the northern end of the transect reached the surface before the southern end did. Erosion continued to the south until the southern end of the transect reached the surface. Figures 6.7 a - e illustrate this.

Figures 6.7 f - j illustrate the model of depressed isotherms. This model appears to be a simpler explanation of the trend in ages because it requires no changes in uplift rates of one end relative to the other. Although Gaudemer et al. (1988) did not discuss erosion of an orogen with depressed isotherms, it is possible that the depressed isotherms would relax as the crust thins. The models represent the peak of the orogenic event, while the muscovite samples provide data for approximately 100 Ma after the peak of the Grenville orogenic event.

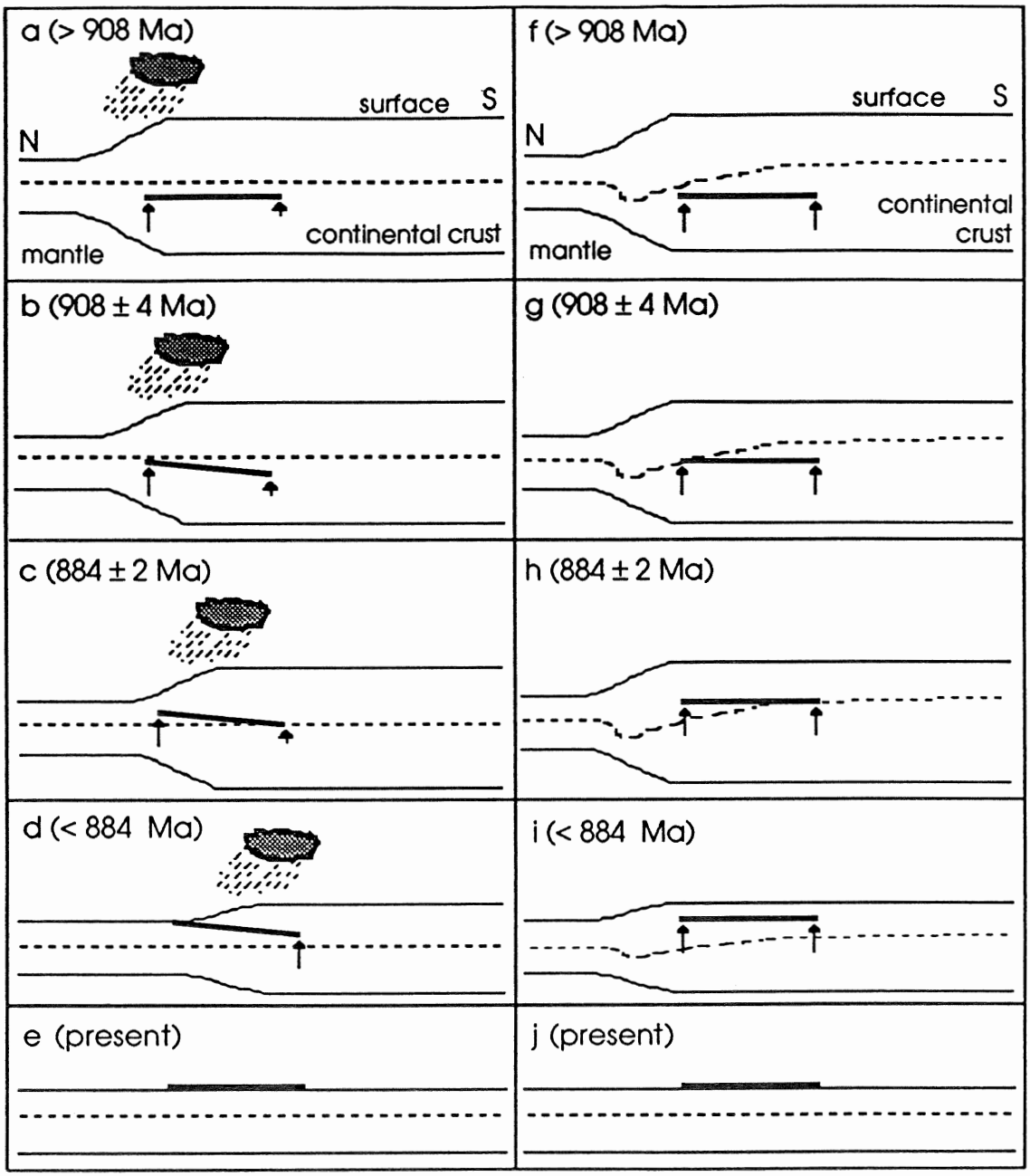

Figure 6.7 Comparison of possible uplift models. a - e: variable uplift, f - j: variable geothermal gradient. Dashed line represents level of muscovite closure temperature. Arrows represent relative rates of uplift. Storm cloud represents area of rapid erosion. N and S indicate north and south, respectively. Thick line represents past position of transect.

CHAPTER 7: CONCLUSIONS

7.1 Ages of Samples

The muscovite ages of the samples in this study range from a high of 908 ±4 Ma in the north, to 884 ±2 Ma in the south. These findings suggest that the muscovite ages obtained by Culshaw et al. (1991) are, on average, 15.5 Ma too old.

The data set, consisting of the recalculated values of Culshaw et al. (1991) and the values of this study, form a trend in ages, perpendicular to the strike of the orogen. This trend may be described as a linear, north to south, decrease in age of samples of 0.23 Ma / km.

7.2 Uplift Models

Both uplift models presented in Chapter 6 explain the trend in ages determined by radiometric dating. Although both models have many assumptions which may never be validated, each one is a plausible explanation of the trend observed.

The model of variable uplift rates is not as simple as it seems initially. In order to satisfy the assumptions of Culshaw et al. (1991), the following series of events must occur. Uplift rates must initially be the same, increase in the north relative to the south, then increase in the south relative to the north. Another problem involves having one end of the transect arrive at the surface and then remain stable for several million years while the other end continues to rise. The pattern of higher erosion rates moving into the interior of the orogen with time may explain these problems.

The model of variable isotherms is a simpler explanation of the trend in ages. Relative uplift rates remain the same throughout, and all samples arrive at the surface at the same time. The problem of why this trend in ages was not observed in the hornblende samples of Culshaw et al. (1991) remains. Temperature-time data indicate that the hornblendes uplifted at a rate significantly greater than that of the muscovites. Therefore, the hornblendes possibly passed through a depressed isotherm representing hornblende closure temperature too quickly for them to record significantly different ages.

Neither model is perfect, but each one offers plausible elements the other lacks. The two models may be viewed as end members of a model which incorporates elements of both. This hybrid model suggests that isotherms were depressed below the frontal thrust zone, and that uplift was greater in the north at first, then greater in the south.

7.3 Future Work

Problems worth investigating in the future include:

development of the hybrid model discussed in the previous section;

obtaining more data, both to the north and south of the study area (not enough is known about the Grenville Front Tectonic Zone); and

the possibility of several cooling paths below 300° C, as suggested by muscovite and K-feldspar data.

REFERENCES

Corrigan D (1990) Geology and U-Pb geochronology of the Key Harbour area, Britt Domain, southwest Grenville Province. MSc thesis, Dept of Geology, Dalhousie Univ, Halifax, N.S.

Cosca MA, Sutter JF, Essene EJ (1990) Late metamorphic cooling and erosion history of the Ontario Grenville Province: constraints from $^{40}Ar/^{39}Ar$ thermochronometry. Tectonics, in press

Culshaw N, Reynolds PH, Check G (1991) A $^{40}Ar/^{39}Ar$ study of post tectonic cooling and uplift in the Britt domain of the Grenville Province, Ontario. Earth Planet Sci Lett, in press

Culshaw NG, Davidson A, Nadeau L (1983) Structural subdivisions of the Grenville Province in the Parry Sound - Algonquin region, Ontario. In: Geological Survey of Canada Paper 83-1B, Minister of Supply and Services Canada, Ottawa, pp 243-251

Culshaw NG, Corrigan D, Drage J, Wallace P (1988) Georgian Bay geological synthesis: Key Harbour to Dillon, Grenville Province of Ontario. In: Geological Survey of Canada Paper 88-1C, Minister of Supply and Services Canada, Ottawa, pp 129-133

Culshaw NG, Check G, Corrigan D, Drage J, Gower R, et al.(1989) Georgian Bay geological synthesis: Dillon to Twelve Mile Bay, Grenville Province of Ontario. In: Geological Survey of Canada Paper 89-1C, Minister of Supply and Services Canada, Ottawa, pp 157-163

Culshaw NG, Corrigan D, Jamieson R, Ketchum J, Wallace P, et al. (1990) Evidence for duplexing and extension in the ductile mid-crust from the Central Gneiss Belt, Grenville Province, Georgian Bay, Ontario. unpublished, Dept of Geology, Dalhousie Univ, Halifax, N.S.

Davidson A (1984a) Identification of ductile shear zones in the southwestern Grenville Province of the Canadian Shield. In: Precambrian Tectonics Illustrated. Kröner A, Greiling, R (eds) Schweitzerbart'sche Verlagbuchhandlung, Stuttgart, pp 263-279

Davidson A (1984b) Tectonic boundaries within the Grenville Province of the Canadian Shield. Journ of Geodynam 1:433-444

Davidson A (1985) Tectonic framework of the Grenville Province in Ontario and western Quebec, Canada. In: The Deep Proterozoic Crust in the North Atlantic Provinces. Tobi AC, Touret JLR (eds) D. Reidel Publishing Co, Dordrecht, pp 133-149

Davidson A (1986) New interpretations in the southwestern Grenville Province. In: The Grenville Province. Moore JM, Davidson A, Baer AJ (eds) GAC Special Paper 31, Geological Association of Canada, St. John's, pp 61-74

Davidson A, van Breemen O (1988) Baddeleyite-zircon relationships in coronitc metagabbro, Grenville Province, Ontario: implications for geochronlogy. Cont Mineral Petrol 100: 291-299

Deer WA, Howie RA, and Zussman J (1966) An introduction to the rock-forming minerals. Longman Group Limited, Essex

Dodson MH (1973) Closure Temperature in Cooling Geochronological and Petrological Systems. Cont Mineral Petrol, 40: 259-274

Easton RM (1986) Geochronology of the Grenville Province. In: The Grenville Province. Moore JM, Davidson A, Baer AJ (eds) GAC Special Paper 31, Geological Association of Canada, St. John's, pp 127-173

Ellsworth (1932) Rare- element minerals of Canada. GSC Economic Geology Report 11

Fleck RJ, Sutter JF, and Elliot DH (1977) Interpretation of discordant $^{40}Ar/^{39}Ar$ age-spectra of Mesozoic tholeiites from Antarctica. Geochim et Cosmochim Acta 41: 15-32

Faure G (1986) Principles of isotope geology. John Wiley & Sons, New York

Gaudemer Y, Jaupart C, and Tapponnier P (1989) Thermal control on post-orogenic extension in collision belts. Earth Planet Sci Lett 89: 48-62

Haugerud RA (1989) On numerical modeling of one-dimensional geothermal histories. Comput and Geosci 15, 5: 825-836

Ketchum J (1991) Metamorphism and structure of the Central Britt Shear Zone, Grenville Province, Ontario. PhD thesis, in prep, Dept of Geology, Dalhousie Univ, Halifax, N.S.

Kretz R (1983) Symbols for rock-froming minerals. Am Mineral 68: 277-279

Lister GS, Boland JN, and Zwart HJ (1986) Step-wise growth of biotite porphyroblasts in pelitic scists of the western Lys_caillaouas massif (Pyrenees). Journ Struct Geol 8,5: 543-562

Logan WE (1863) Report on the geology of Canada. In: Geological Survey of Canada, report of progress from its commencement to 1863

Logan WE (1847) Report of progress for the year 1845-6. Geological Survey of Canada, p 1-98

McDougall I and Harrison TM (1988) Geochronology and Thermochronology by the $^{40}Ar/^{39}Ar$ Method. Oxford Univ Press, Inc, New York

Moore JM (1986) Introduction: The 'Grenville Problem' Then and Now. In: The Grenville Province. Moore JM, Davidson A, Baer AJ (eds) GAC Special Paper 31, Geological Association of Canada, St. John's, pp 1-12

Petrucci RH (1985) General chemistry. Macmillan Publishing Co, New York

Purdy JW, Jäger E (1976) K-Ar ages on rock-forming minerals from the central Alps. Mem 1st Geol Min Univ Padova 30: 31 pp

Rivers T, Davidson A, Gower CF, Martignole J (1989) New tectonics of the Grenville Province, southeast Canadian Shield. Tectonics 8,1: 63-84

Sharma PV (1986) Geophysical methods in geology. Elsevier Publishing Co, Inc, New York

Skinner BJ, Porter, SC (1987) Physical geology. John Wiley and Sons, New York

Snee LW, Sutter JF, and Kelley WC (1988) Thermochronology of economic mineral deposits: dating the satges of mineralization at Panasqueira, Portugal, by high-precision $^{40}Ar/^{39}Ar$ age spectrum techniques on muscovite. Econ Geol 83: 335-354

van Breemen O, Davidson A, Loveridge WD, Sullivan RW (1986) U-Pb zircon geochronology of Grenville tectonites, granulites and igneous precursors, Parry Sound, Ontario. In: The Grenville Province. Moore JM, Davidson A, Baer AJ (eds) GAC Special Paper 31, Geological Association of Canada, St. John's, pp 191-207

Wynne-Edwards HR (1972) The Grenville Province. In: Variations in Tectonic Styles in Canada. Price RA, Douglas RJW (eds) GAC Special Paper 11, Geological Association of Canada, Montréal, pp 263-334

APPENDIX 1: SAMPLE SITES

Sample #:	Code Name:	Location:
1	88 G404	Key Harbour, Key Harbour gneiss association
2	87DMG DO14b	Key River, Key Harbour gneiss association
3	88 G7b	Henvey Inlet, Key Harbour gneiss association
4	87DMG N56	Golden Sword Island, Key Harbour gneiss association
5	87DMG N202	Norgate Inlet, Key Harbour gneiss association
6	H Lk Rd	Highway 69, north of Harris Lake Road, metasedimentary part of Bayfield gneiss association
7	90DMG Nc529a	100 m south of Highway 529a garbage dump, narrow band of metasediment in Bayfield gneiss association
8	90DMG Nc193a	south side of Pointe Au Baril channel, metasediment of Nadeau Island gneiss association
9	87 DMG N428	Nadeau Island, quartz-rich paragneiss of Sand Bay gneiss association
10	87DMG P196	bush locality within Sand Bay gneiss association
11	90DMG Nc210	140 m north-west of Sand Bay and Killbear Roads intersection, Sand Bay gneiss association
12	89DMG SH7a	1 km south of Nobel post office on Highway 69, Lighthouse gneiss association

Sample #:	Code Name:	Location:
13	88DMG Nb160	island on southeast shore of Depot Harbour Inlet, Lighthouse gneiss association
14	88 DMG Nb397a	island north-west of Sandy Island, Sand Bay gneiss association

APPENDIX 2: SAMPLE PETROGRAPHY

The major minerals of the quartzofeldspathic gneisses are quartz, feldspar(s), and mica(s). Quartzofeldspathic pelitic gneisses may also contain corundum and/or garnet. Schists contain large percentages of micas, obvious in both hand specimen and thin section. Migmatitic samples contain up to 60% leucosome.

Modal percentages and grain sizes are approximations.

Commonly, grains occur in distinct groups of discontinuous size ranges. These "grain size families" are noted only for muscovite.

Tabular muscovite grains are short and blocky with a minimal number of sides. Radiator-fin muscovite grains (Lister 1986) tend to be longer, and have jagged ends which fit into other grains in a manner similar to jig-saw puzzle pieces. Muscovite grains with regular, straight boundaries are decussate. Photomicrographs show examples of these characteristics.

In cases where the variety of feldspars is too great, or the sizes are too small, to accurately distinguish types and abundances, the feldspars are grouped. "Others" indicates all other minerals which, in total, account for less than 5% of the sample. Mineral abbreviations are after Kretz (1983).

Figure A2.1 Photograph of hand specimens 2, 4 - 8, and 10 -13. Specimens 1, 3, 9, and 14 were not available.

Rock Type:	quartzofeldspathic pelitic gneiss alternating Bt-Ms-rich layers, Ms-rich layers, and Afs-rich layers		
Minerals:	Modal %:	Grain Size:	Grain Size Families:
muscovite	60	0.5 - 3 mm	0.5 - 1 mm, 2 - 3 mm
feldspars	10	0.5 - 1 mm	
quartz	10	0.5 - 1 mm	
opaques	10	0.5 - 2 mm	
biotite	5	~ 2 mm	
corundum	5	0.5 - 1 mm	
others	< 1	variable	
Muscovite Comments:	well-defined contacts with biotite undulose extinction radiator-fin grains some appears to be altered (sericite?) inconsistent birefringence across grains		

Table A2.1 Petrography of sample 1.

Rock Type:	quartzofeldspathic pelitic gneiss alternating Ms-rich and feldspar-rich layers	
Minerals:	Modal %:	Grain Size:
muscovite	50	1 - 2 mm
quartz	10	1 - 2 mm
microcline	10	1 - 2 mm
plagioclase	5	1 - 2 mm
other feldspars	10	1 - 2 mm
corundum	10	< 0.5 mm
others	5	variable
Muscovite Comments:	tabular grains some display decussate texture	

Table A2.2 Petrography of sample 2.

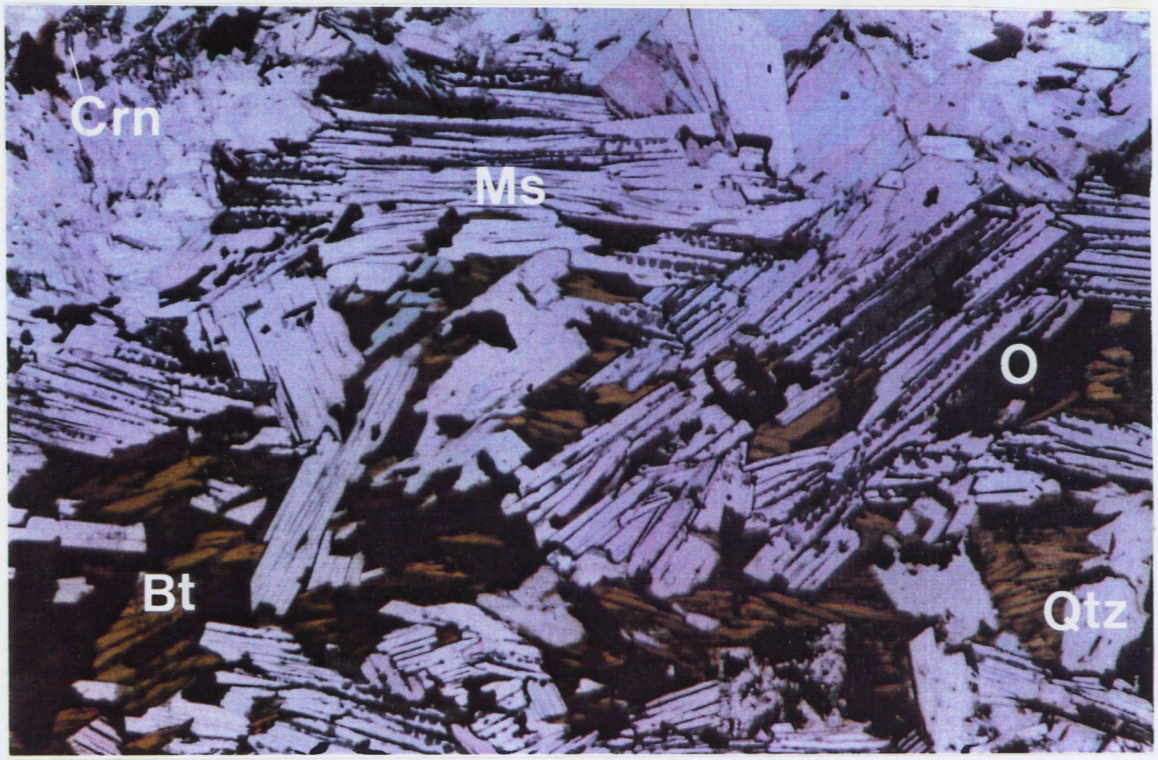

Figure A2.2 Photomicrograph of sample 1.
Field of view: ~ 7 mm.
Light: plane polarized.
Tungsten filter used.
Ms: muscovite.
Qtz: quartz.
O: opaques.
Bt: biotite.
Crn: corundum.

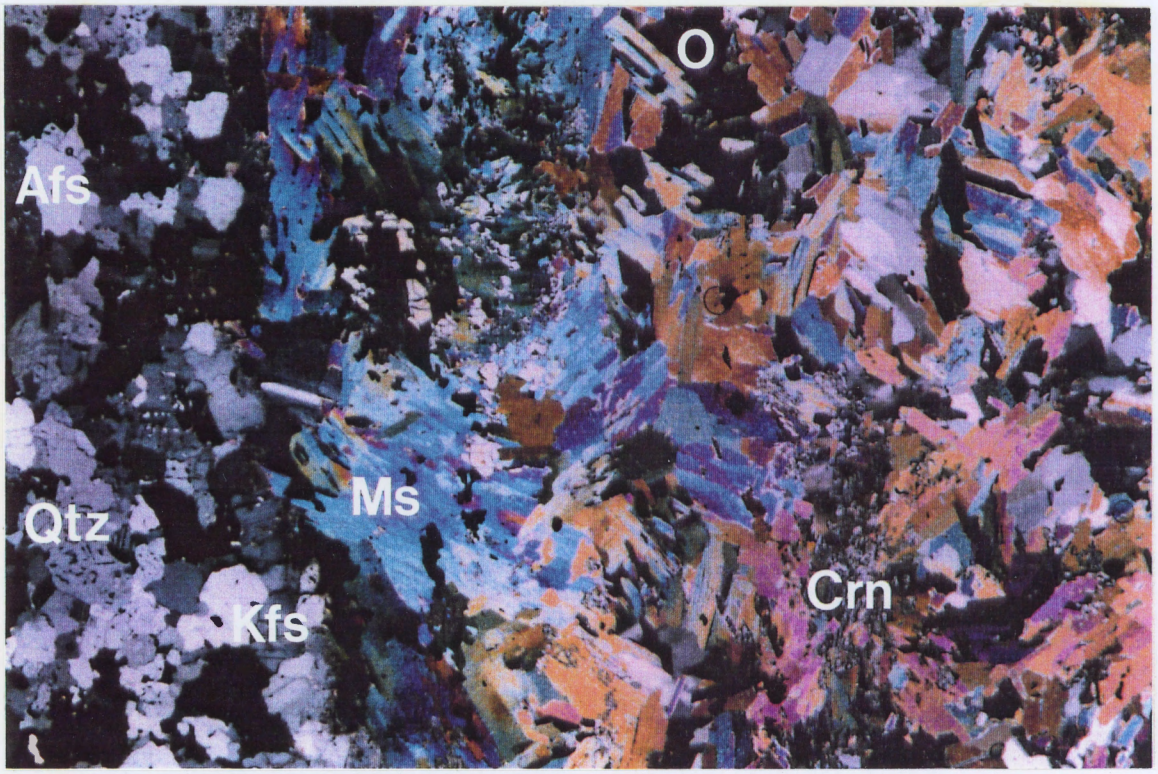

Figure A2.3 Photomicrograph of sample 2.
Field of view: ~ 10 mm.
Light: cross polarized.
Tungsten filter used.
Boundary between muscovite-rich layer and feldspar-rich layer at left.
Ms: muscovite.
Qtz: quartz.
Afs: alkali feldspars.
Kfs: K-feldspars.
Crn: corundum.
O: opaques.

Rock Type:	quartzofeldspathic gneiss alternating Ms-rich and feldspar-rich layers
Minerals:	**Modal %:**	**Grain Size:**
muscovite	40	1 - 3 mm
microcline	45	1 - 2 mm
other feldspars	5	< 1 m
others (including biotite, quartz, chlorite and plagioclase)	10	variable
Muscovite Comments:	tabular grains some grains have decussate texture

Table A2.3 Petrography of sample 3.

Rock Type:	quartzofeldspathic gneiss
Minerals:	**Modal %:**	**Grain Size:**
quartz	35	0.5 - 2 mm
plagioclase	15	< 1 mm
other feldspars	30	0.5 - 2 mm
muscovite	5	0.1 - 3 mm
kyanite	5	0.1 - 2 mm
opaques	5	< 0.5 mm
others (including kyanite)	5	variable
Muscovite Comments:	very few muscovite-muscovite contacts

Table A2.4 Petrography of sample 4.

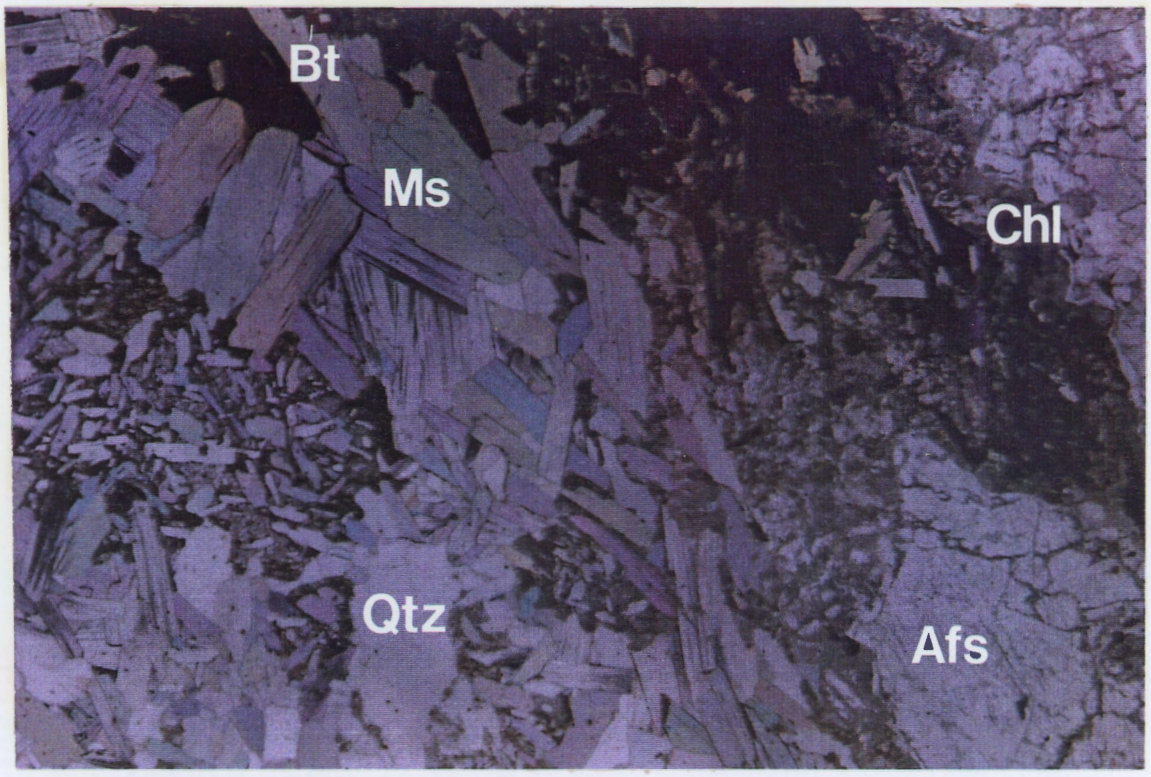

Figure A2.4 Photomicrograph of sample 3.
Field of view: ~ 14 mm.
Light: partially cross polarized.
Tungsten filter used.
Good example of tabular muscovite grains with decussate muscovite-muscovite boundaries.
Ms: muscovite.
Afs: alkali feldspars.
Bt: biotite.
Qtz: quartz.
Chl: chlorite.

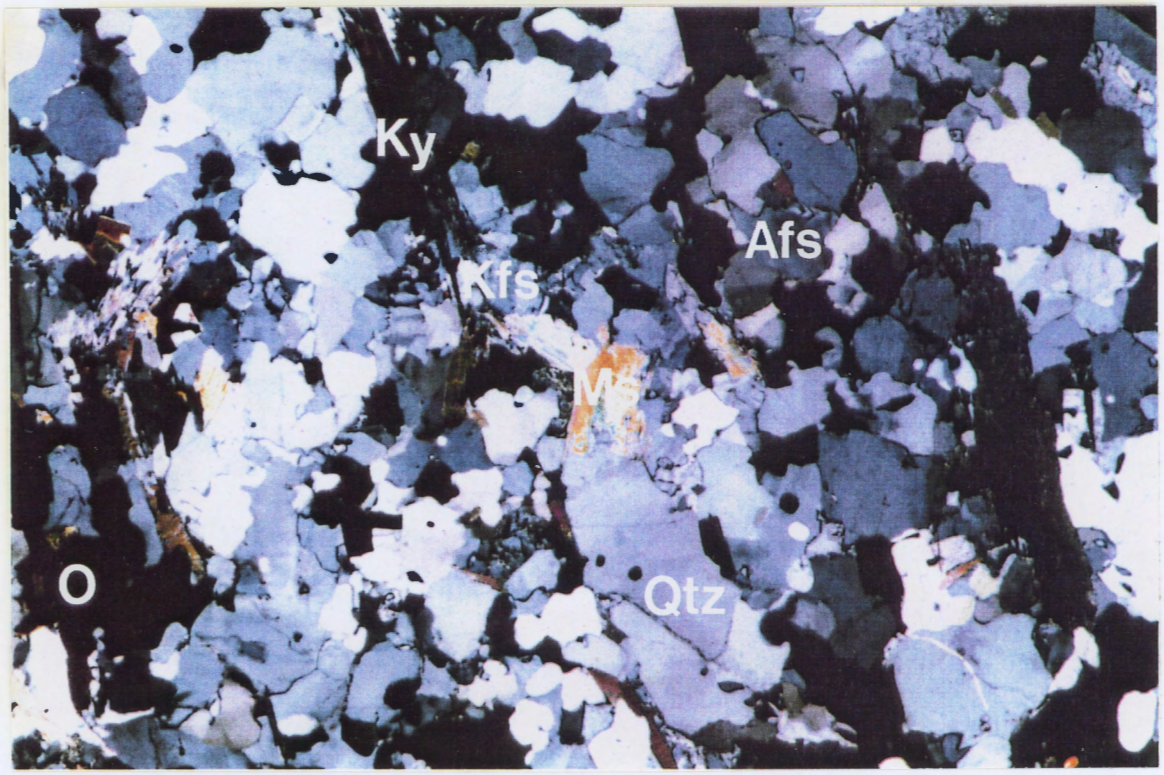

Figure A2.5 Photomicrograph of sample 4.
Field of view: ~ 6.5 mm.
Light: cross polarized.
Tungsten filter used.
Kfs: K-feldspars.
Ms: muscovite.
O: opaques.
Ky: kyanite.
Qtz: quartz.
Afs: alkali feldspars.

Rock Type:	quartzofeldspathic gneiss	
Minerals:	Modal %:	Grain Size:
plagioclase	40	0.5 - 2 mm
microcline	40	0.5 - 2 mm
biotite	10	1 - 2 mm
muscovite	5	< 1 mm
others (including quartz)	5	variable
Muscovite Comments: very little deformation		

Table A2.5 Petrography of sample 5.

Rock Type:	quartzofeldspathic migmatitic gneiss	
Minerals:	Modal %:	Grain Size:
quartz	50	0.5 - 3 mm
microcline	30	0.5 - 1 mm
other feldspars	5	< 0.5 mm
biotite	10	1 - 2 mm
muscovite	5	1 - 3 mm
others (including chlorite and opaques)	< 1	variable
Muscovite Comments:	intergrown with feldspars no decussate textures	

Table A2.6 Petrography of sample 6.

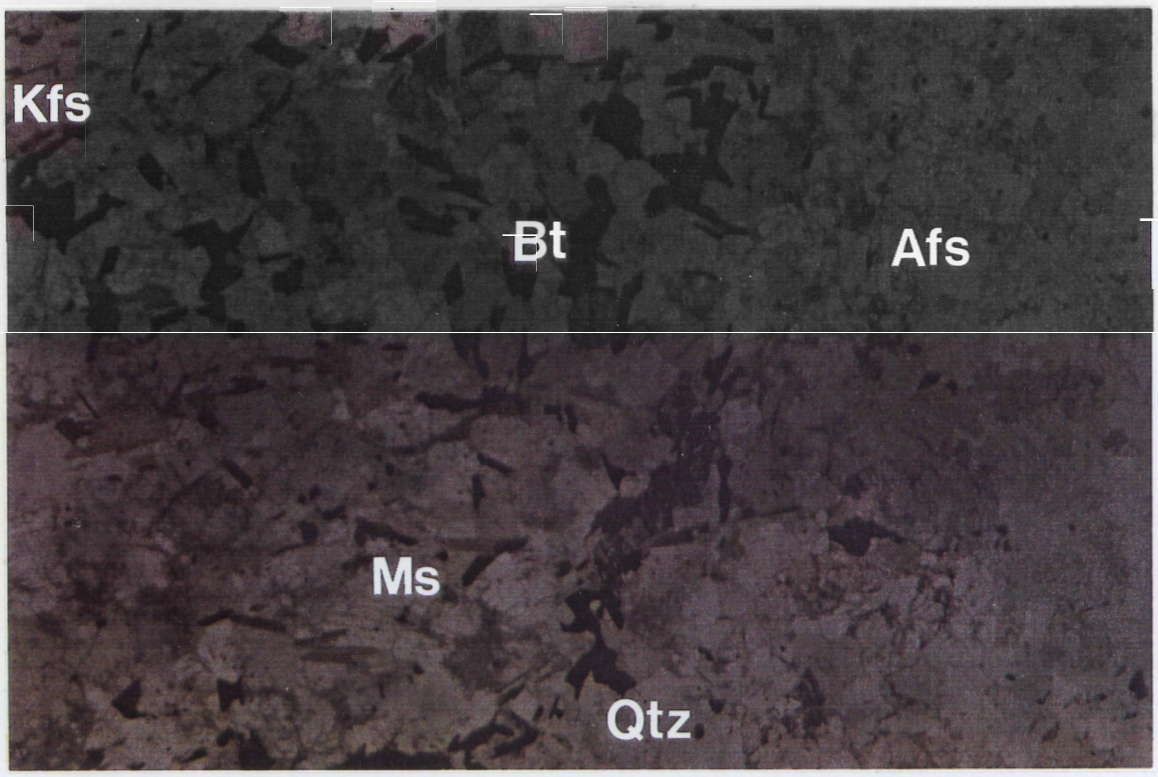

Figure A2.6 Photomicrograph of sample 5.
Field of view: ~ 13 mm.
Light: plane polarized.
Tungsten filter used.
Kfs: K-feldspars.
Afs: alkali feldspars.
Bt: biotite.
Ms: muscovite.
Qtz: quartz.

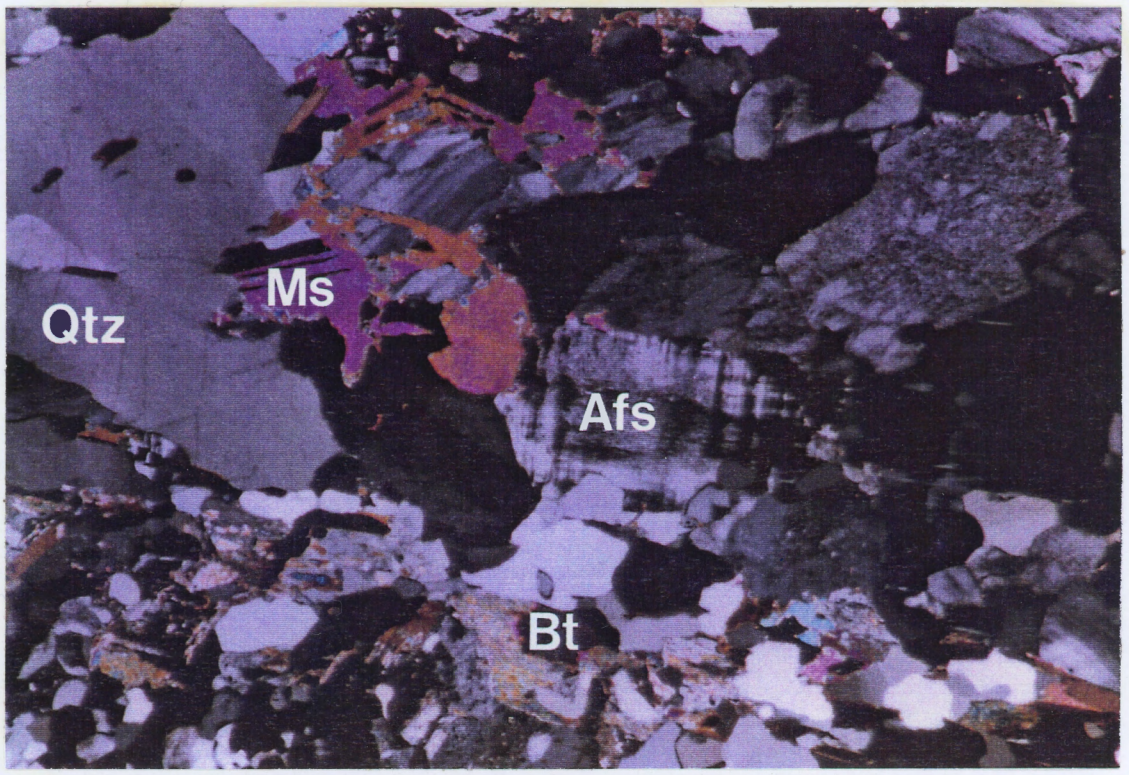

Figure A2.7. Photomicrograph of sample 6.
Field of view: ~ 5 mm.
Light: cross polarized.
No tungsten filter used.
Qtz: quartz.
Afs: alkali feldspars.
Bt: biotite.
Ms: muscovite.

Rock Type:	quartzofeldspathic pelitic gneiss alternating Ms-rich and feldspar-rich layers	
Minerals:	Modal %:	Grain Size:
muscovite	45	0.5 - 3 mm
plagioclase	20	0.5 - 3 mm
other feldspars	20	0.5 - 3 mm
biotite	10	1 - 2 mm
garnet	5	1 mm
others (including quartz)	< 1	variable
Muscovite Comments:	tabular grains most have decussate texture	

Table A2.7 Petrography of sample 7.

Rock Type:	schist		
Minerals:	Modal %:	Grain Size:	Grain Size Families:
muscovite	35	1 - 3 mm	~ 1 mm, 3 - 4 mm
plagioclase	35	1 - 2 mm	
biotite	20	0.5 - 2 mm	
opaques	5	0.5 - 2 mm	
others	5	variable	
Muscovite Comments:	clustered in places (glomeroporphyritic) tabular grains good decussate texture		

Table A2.8 Petrography of sample 8.

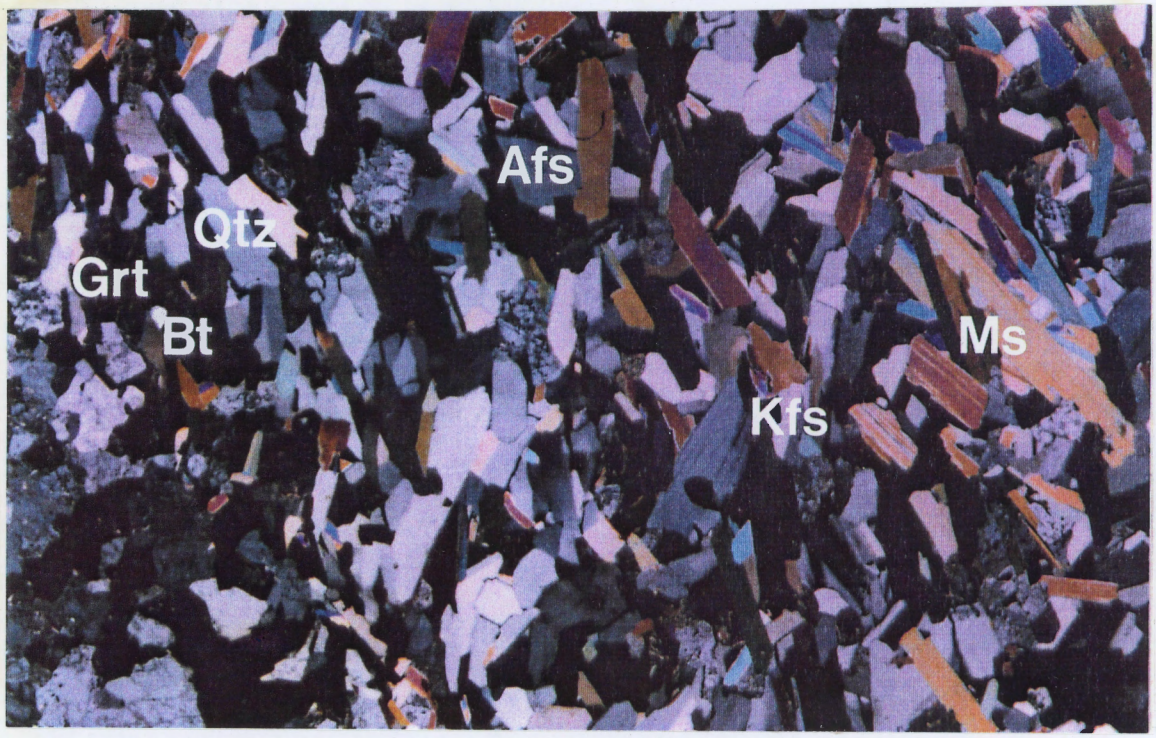

Figure A2.8 Photomicrograph of sample 7.
Field of view: ~ 18 mm.
Light: cross polarized.
Tungsten filter used.
Good example of tabular grains with decussate texture.
Ms: muscovite.
Kfs: K-feldspars.
Afs: alkali feldspars.
Bt: biotite.
Grt: garnet.
Qtz: quartz.

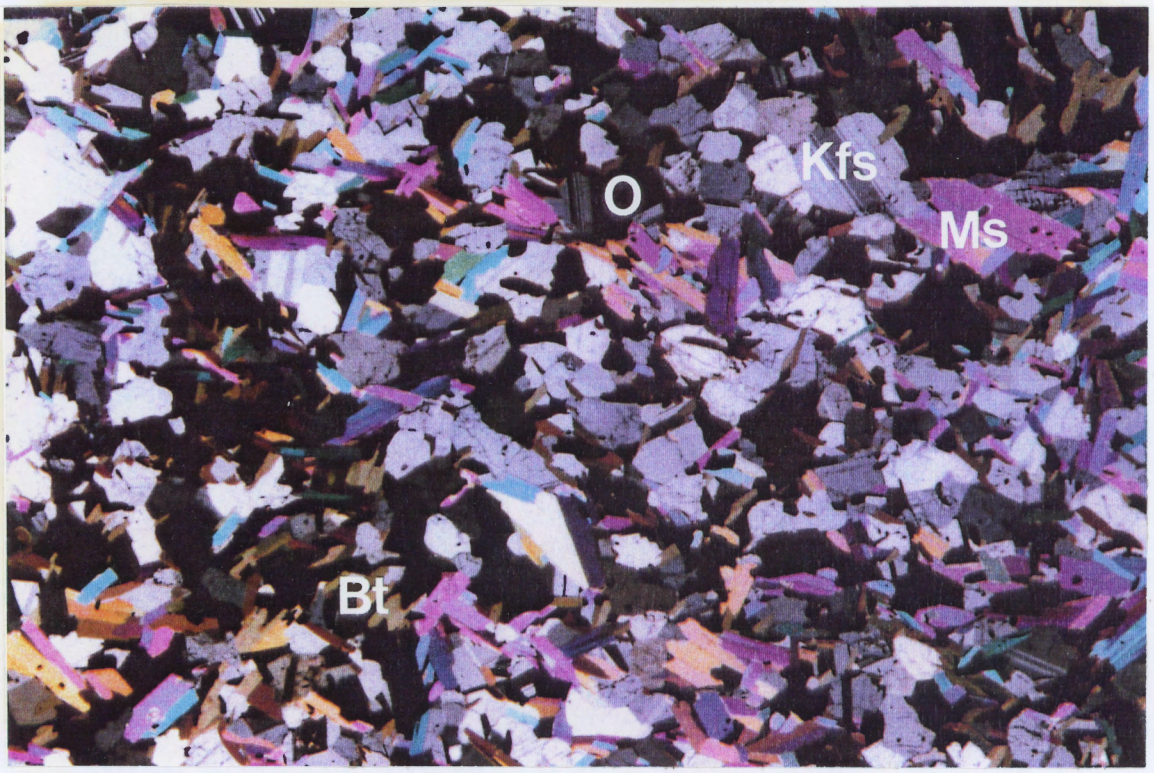

Figure A2.9 Photomicrograph of sample 8.
Field of view: ~ 12.5 mm.
Light: cross polarized.
Tungsten filter used.
Ms: muscovite.
Kfs: K-feldspars.
Bt: biotite.
O: opaques.

Rock Type:	quartzofeldspathic gneiss	
Minerals:	Modal %:	Grain Size:
K-feldspars	40	1 - 4 mm
quartz	40	1 - 4 mm
muscovite	15	1 - 3 mm
biotite	5	0.5 - 1 mm
others (including kyanite and corundum)	< 1	variable
Muscovite Comments: very few muscovite-muscovite contacts		

Table A2.9 Petrography of sample 9.

Rock Type:	quartzofeldspathic gneiss	
Minerals:	Modal %:	Grain Size:
quartz	50	0.5 - 3 mm
microcline	15	< 1 mm
other feldspars	5	< 1 mm
muscovite	15	0.5 - 2 mm
biotite	10	0.5 - 1 mm
others	5	variable
Muscovite Comments:	intergrown with feldspars tabular and radiator-fin grains	

Table A2.10 Petrography of sample 10.

Figure A2.10 Photomicrograph of sample 9.
Field of view: ~ 14 mm.
Light: cross polarized.
No tungsten filter used.
Quartz displays anomalously high interference colours (section may be too thick).
Afs: alkali feldspars.
Qtz: quartz.
Ms: muscovite.
O: opaques.

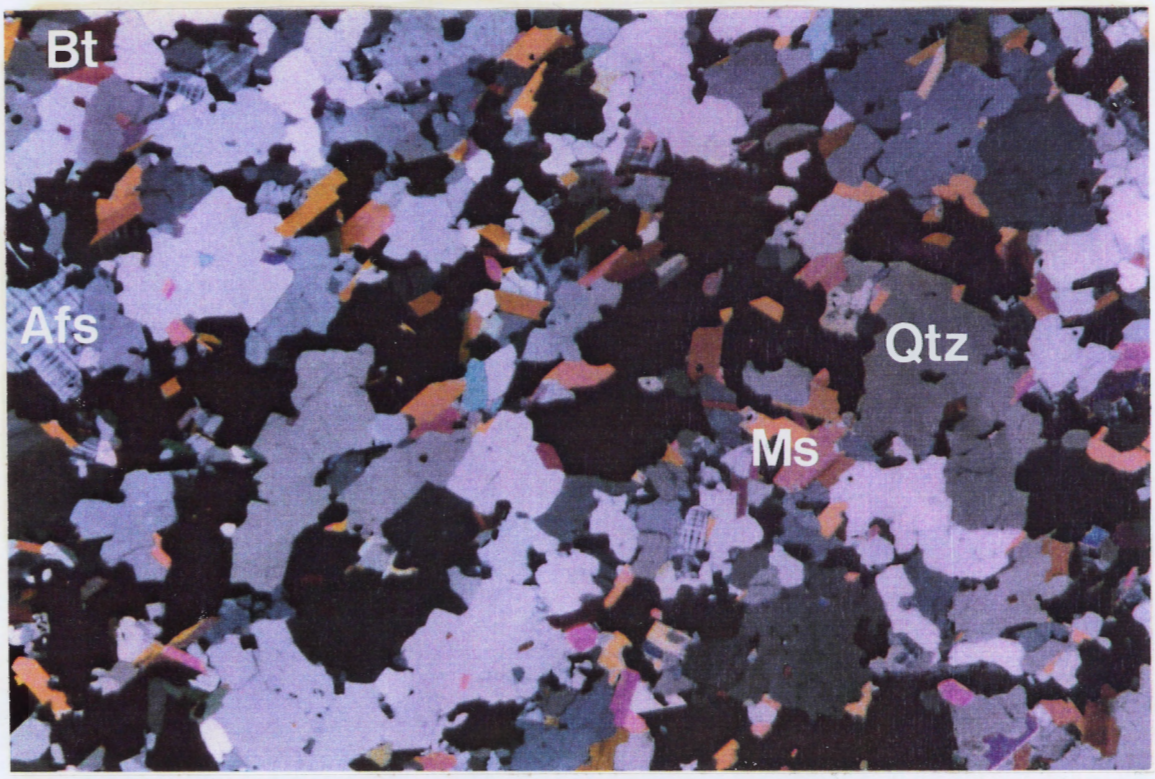

Figure A2.11 Photomicrograph of sample 10.
Field of view: ~ 9 mm.
Light: cross polarized.
Tungsten filter used.
Qtz: quartz.
Afs: alkali feldspars.
Ms: muscovite.
Bt: biotite.

Rock Type:	quartzofeldspathic gneiss alternating Ms-rich and feldspar-rich layers
Minerals:	Modal %: Grain Size:
quartz	40 1 - 3 mm
muscovite	25 1 - 3 mm
feldspars	20 1 - 4 mm
biotite	10 1 - 2 mm
others	5 variable
Muscovite Comments:	inclusions, including hematite tabular and radiator-fin grains

Table A2.11 Petrography of sample 11.

Rock Type:	schist foliation defined by micas
Minerals:	Modal %: Grain Size:
muscovite	30 1 - 3 mm
biotite	30 1 - 3 mm
feldspars	15 0.5 - 2 mm
quartz	15 1 - 3 mm
garnet	10 1 - 4 mm
others	< 1 variable
Muscovite Comments:	lineated, bent around other grains very long grains opaque inclusions

Table A2.12 Petrography of sample 12.

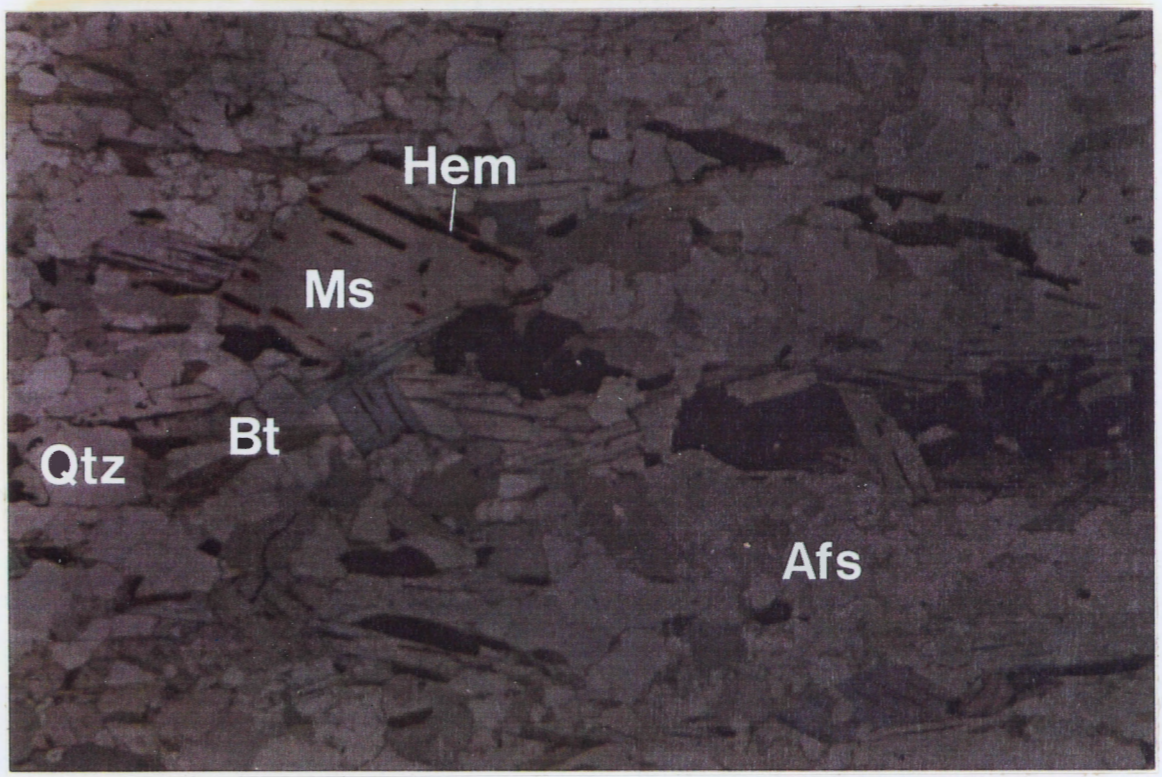

Figure A2.12 Photomicrograph of sample 11.
Field of view: ~ 9 mm.
Light: plane polarized.
Tungsten filter used.
Qtz: quartz.
Ms: muscovite.
Afs: alkali feldspars.
Bt: biotite.
Hem: hematite.

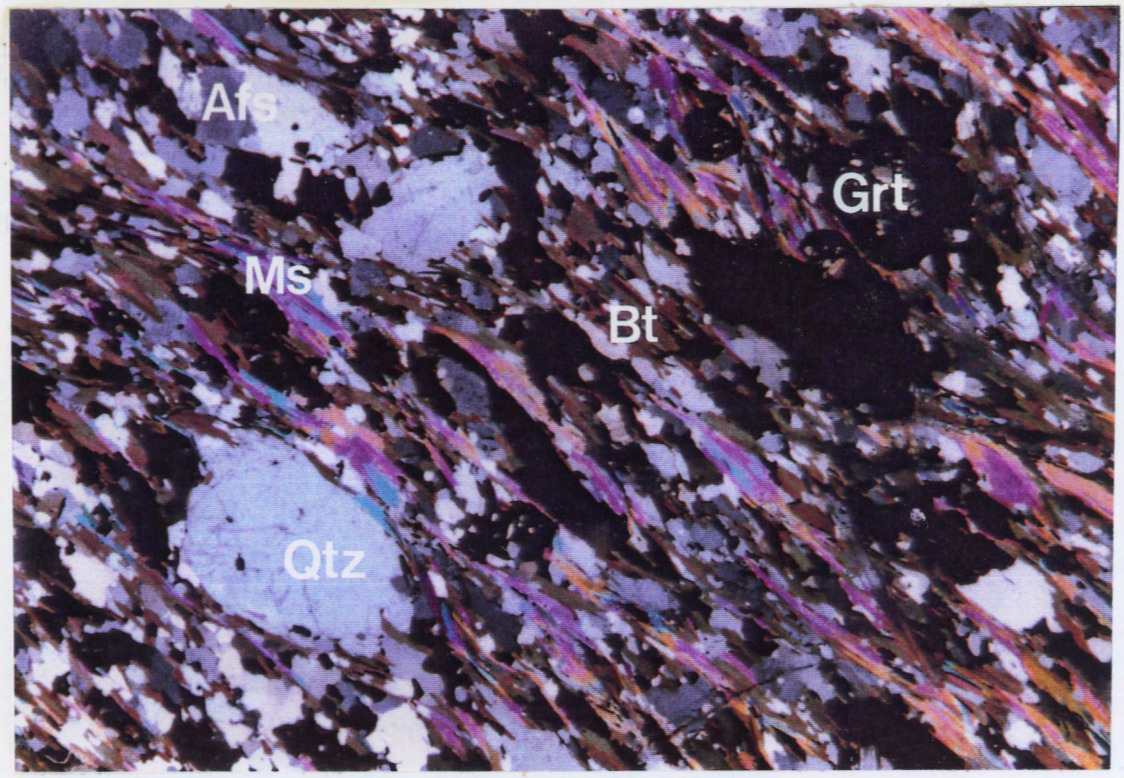

Figure A2.13 Photomicrograph of sample 12.
Field of view: ~ 9.5 mm.
Light: cross polarized.
Tungsten filter used.
Ms: muscovite.
Bt: biotite.
Afs: alkali feldspars.
Qtz: quartz.
Grt: garnet.

Rock Type:	schist	
	foliation defined by micas (crenulated)	
Minerals:	Modal %:	Grain Size:
muscovite	30	0.1 - 5 mm
feldspars	15	0.5 - 3 mm
quartz	15	0.5 - 2 mm
biotite	20	1 - 3 mm
garnet	15	2 - 4 mm
others (including chlorite, staurolite, and opaques)	5	variable
Muscovite Comments:	lineated, bends around other grains	
	displays high relief	
	very long grains	
	radiator-fin grains	

Table A2.13 Petrography of sample 13.

Rock Type:	quartzofeldspathic gneiss	
	alternating Ms-rich and Ms-poor layers	
Minerals:	Modal %:	Grain Size:
quartz	40	0.5 - 2 mm
biotite	20	< 1 mm
plagioclase	15	< 0.5 mm
other feldspars	10	< 1 mm
muscovite	10	0.1 - 2 mm
others	5	variable
Muscovite Comments:	very long grains	
	radiator-fin grains	
	grains form lineation	

Table A2.14 Petrography of sample 14.

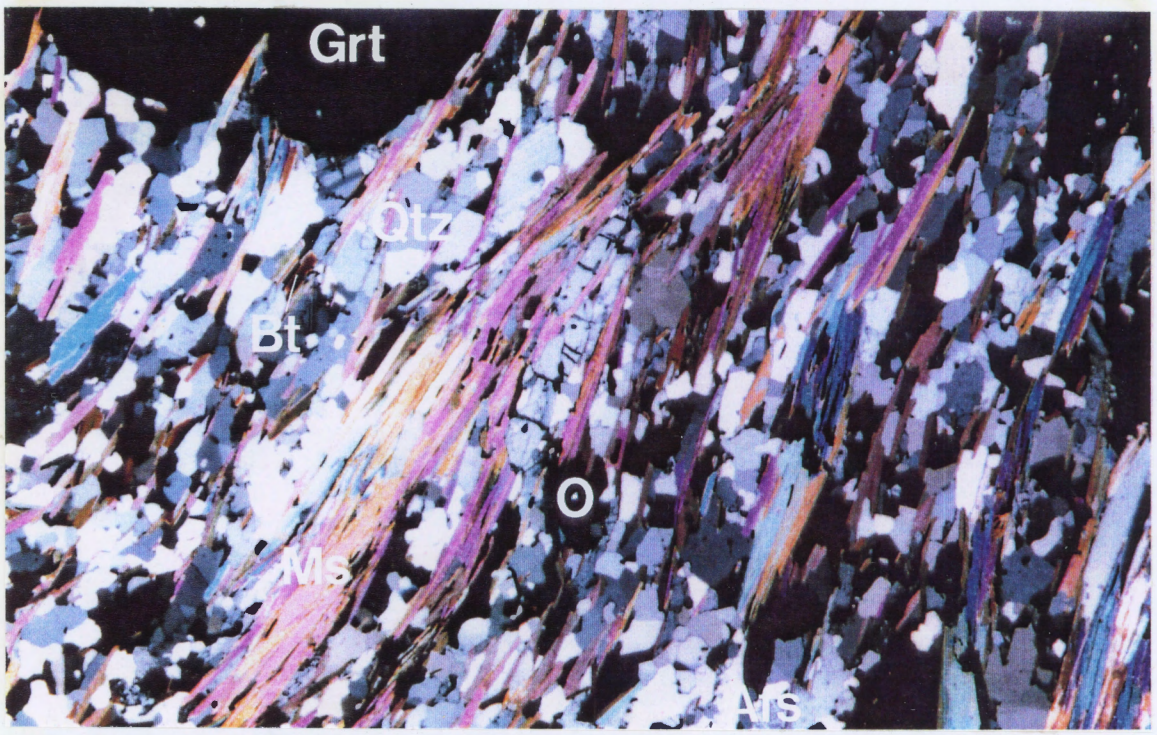

Figure A2.14 Photomicrograph of sample 13.
Field of view: ~ 9 mm.
Light: plane polarized.
Tungsten filter used.
Ms: muscovite.
Afs: alkali feldspars.
Qtz: quartz.
Bt: biotite.
Grt: garnet.
O: opaques.

Figure A2.15 Photomicrograph of sample 14.
Field of view: ~ 16 mm.
Light: cross polarized.
No tungsten filter used.
A good example of radiator-fin texture is in the lower right corner.
Qtz: quartz.
Bt: biotite.
Kfs: K-feldspars.
Afs: alkali feldspars.
Ms: muscovite.

APPENDIX 3: MATHEMATICAL FORMULAE

The basic equation of geochronology, as outlined by McDougall and Harrison (1988), is derived as follows.

Because a radioactive element decays in an exponential manner, the number of radioactive atoms present at any time may be expressed as

$$dN/dt = -\lambda N \qquad (A3.1)$$

where N is the number of radioactive atoms present at time t and λ is the decay constant of that isotope. The half life, $t_{1/2}$, of the radioactive element may be expressed as

$$t_{1/2} = (\ln 2) / \lambda = 0.693 / \lambda \qquad (A3.2)$$

Equation A3.2 may be rearranged and integrated as

$$N = N_o \exp(-\lambda t) \qquad (A3.3)$$

where N_o is the number of radioactive atoms present at time t (a time in the past).

If a parent isotope decays to a daughter isotope, then

$$N_o = N + D \qquad (A3.4)$$

where N is the number of parent atoms and D is the number of daughter atoms. Equation A3.4 may be substituted into equation A3.3 to obtain

$$N = (N + D) \exp(-\lambda t) \qquad (A3.5)$$

This equation may be rearranged and its natural logs taken to obtain

$$t = \frac{1}{\lambda} \ln (1 + D/N) \qquad \text{(A3.6)}$$

This is the basic equation of geochronology. It may then be solved by substituting measured values for D and N to obtain t, the age of the sample.

Faure (1986) outlines the mathematical equations related to the $^{40}Ar/^{39}Ar$ dating method. Some of these follow.

The production of ^{39}Ar by the irradiation of ^{39}K may be expressed as

$$^{39}Ar = {}^{39}K\Delta T \int \varphi(\varepsilon)\, \sigma(\varepsilon)\, d\varepsilon \qquad \text{(A3.7)}$$

where ^{39}Ar is the number of ^{39}Ar atoms produced, ^{39}K is the number of ^{39}K atoms irradiated, ΔT is the irradiation time, $\varphi(\varepsilon)$ is the "neutron flux density at energy ε," and $\sigma(\varepsilon)$ is the "capture cross section of ^{39}K for neutrons having energy ε" (Faure 1986, p 93). The limits of integration are the entire energy spectrum of the neutrons.

The decay of ^{40}K to ^{40}Ar may be expressed as

$$^{40}Ar^{*} = \lambda_{\kappa}/\lambda\, {}^{40}K(e^{\lambda t}-1) \qquad \text{(A3.8)}$$

where $^{40}Ar^{*}$ is the number of radiogenic ^{40}Ar atoms produced, ^{40}K is the number of ^{40}K atoms initially present, λ_{κ} is the ^{40}K electron capture constant, λ is the total ^{40}K decay constant, and t is the age of the sample.

By dividing (A3.8) by (A3.7), the $^{40}Ar/^{39}Ar$ ratio may be obtained:

$$\frac{^{40}Ar^*}{^{39}Ar} = \frac{\lambda_\kappa \ ^{40}K \ (e^{\lambda t}-1)}{\lambda \ ^{39}K \ \Delta T \int \varphi(\varepsilon) \, \sigma(\varepsilon) \ d\varepsilon} \qquad \text{(A3.9)}$$

A parameter, J, may be introduced to express some of the variables which are difficult to evaluate:

$$J = \frac{\lambda \ ^{39}K \ \Delta T \int \varphi(\varepsilon) \, \sigma(\varepsilon) \ d\varepsilon}{\lambda_\kappa \ ^{40}K} \qquad \text{(A3.10)}$$

Substituting (A3.10) into (A3.9) yields

$$\frac{^{40}Ar^*}{^{39}Ar} = \frac{e^{\lambda t}-1}{J} \qquad \text{(A3.11)}$$

If a sample of known age is irradiated along with the others, J may be determined by

$$J = \frac{e^{\lambda tm} - 1}{^{40}Ar^*/^{39}Ar} \qquad \text{(A3.12)}$$

where tm is the known age of the sample and $^{40}Ar^*/^{39}Ar$ is the measured value for this sample.

Equation A3.11 may be rearranged as

$$t = 1/\lambda \ \ln \ ((^{40}Ar^*/^{39}Ar) \ J + 1) \qquad \text{(A3.13)}$$

After inserting the value of J determined with (A3.12), the age of each unknown sample may be calculated by inserting its measured $^{40}Ar^*/^{39}Ar$ ratio. The error in t, σt, may be expressed as

$$\sigma t \approx \left[\frac{J^2 \ F^2 \ (\sigma F^2 + \sigma J^2)}{t^2 \lambda^2 \ (1 + FJ)^2}\right]^{1/2} \qquad \text{(A3.14)}$$

where "F = $^{40}Ar^*/^{39}Ar$, σF^2 and σJ^2 are the variances of F and J, respectively, expressed in percent, t is the age of the sample, and λ is the total decay constant of ^{40}K" (Faure 1986, p 94).

A simpler way of calculating the error in t is to base it on the error in J. The relationship between t and J is assumed to be approximately linear, so the error in t is calculated proportionately to the error in J (Reynolds 1991, pers comm).

APPENDIX 4: ANALYSIS SUMMARIES

GD-D4-88 MUSCOVITE SUMMARY

°C	mV 39	% 39	AGE(Ma)	% ATMOS	37/39	40/36	39/36	% IIC
650	29	4	877 +/- 1	9	-	3338	12.1	-
680	18	3	921 +/- 1	3	-	9173	33.2	-
710	15	2	925 +/- 2	2	-	13316	48.5	-
740	36	5	921 +/- 1	3	-	11204	40.8	-
770	36	5	925 +/- 3	2	-	15680	57.3	-
800	121	18	926 +/- 1	2	-	12128	44	-
830	24	4	923 +/- 1	1	-	24166	89.1	-
860	150	23	922 +/- 1	1	-	20076	73.9	-
890	70	11	922 +/- 2	2	-	12562	45.8	-
920	42	6	923 +/- 3	3	-	10097	36.6	-
950	47	7	927 +/- 3	5	-	5522	19.3	-
1000	33	5	916 +/- 4	11	-	2665	8.9	-
1050	24	4	911 +/- 1	19	-	1588	4.9	-
1100	20	3	901 +/- 2	30	-	976	2.6	-

TOTAL GAS AGE = 920 Ma

J = 2.495E-03

ERROR ESTIMATES AT ONE SIGMA LEVEL

37/39,40/36 AND 39/36 Ar RATIOS ARE CORRECTED FOR INTERFERING ISOTOPES

% IIC - INTERFERING ISOTOPES CORRECTION

Table A4.1 Analysis summary for sample 1.

DMB-DO14B-87 MUSCOVITE SUMMARY

°C	mV 39	% 39	AGE(Ma)	% ATMOS	37/39	40/36	39/36	% IIC
740	78	2	-	-	-	-	-	-
770	32	<1	611 +/- 7	22	-	1344	5.9	-
800	25	<1	713 +/- 7	11	-	2726	11.5	-
830	50	1	716 +/- 4	6	-	5010	22.2	-
860	36	<1	779 +/- 2	5	-	6215	25.2	-
890	86	2	759 +/- 3	2	-	13893	59.8	-
920	73	2	917 +/- 3	2	-	15367	52.3	-
950	66	2	915 +/- 2	2	-	14615	49.8	-
980	156	4	913 +/- 2	2	-	17937	61.6	-
1010	405	10	905 +/- 2	2	-	17822	61.9	-
1040	770	18	908 +/- 2	2	-	15484	53.4	-
1070	938	22	905 +/- 2	2	-	13947	48.2	-
1100	790	19	879 +/- 3	2	-	14570	52.3	-
1130	333	8	904 +/- 2	<1	-	33525	117.6	-
1160	199	5	908 +/- 2	1	-	20959	72.7	-
1190	132	3	908 +/- 2	2	-	15638	53.9	-

J = 2.303E-03

ERROR ESTIMATES AT ONE SIGMA LEVEL

37/39,40/36 AND 39/36 Ar RATIOS ARE CORRECTED FOR INTERFERING ISOTOPES

% IIC - INTERFERING ISOTOPES CORRECTION

Table A4.2 Analysis summary for sample 2.

G7B-88 MUSCOVITE SUMMARY

°C	mV 39	% 39	AGE(Ma)	% ATMOS	37/39	40/36	39/36	% IIC
650	35	5	863 +/- 1	9	-	3279	12.1	-
680	10	1	914 +/- 2	3	-	11362	41.8	-
710	7	<1	927 +/- 3	2	-	12358	44.7	-
740	110	15	924 +/- 1	<1	-	33678	124.4	-
770	248	34	923 +/- 1	<1	-	62714	232.9	-
800	51	7	924 +/- 11	<1	-	45211	167.6	-
830	88	12	920 +/- 2	<1	-	34870	129.7	-
860	37	5	925 +/- 3	1	-	22682	83.4	-
890	25	3	921 +/- 1	2	-	12296	44.9	-
930	43	6	919 +/- 2	3	-	8900	32.3	-
970	30	4	916 +/- 1	6	-	5075	18	-
1010	25	3	917 +/- 1	8	-	3927	13.6	-
1150	25	3	898 +/- 2	30	-	989	2.6	-

TOTAL GAS AGE = 919 Ma

J = 2.495E-03

ERROR ESTIMATES AT ONE SIGMA LEVEL

37/39,40/36 AND 39/36 Ar RATIOS ARE CORRECTED FOR INTERFERING ISOTOPES

% IIC - INTERFERING ISOTOPES CORRECTION

Table A4.3 Analysis summary for sample 3.

DMB-N56-87 MUSCOVITE SUMMARY

°C	mV 39	% 39	AGE(Ma)	% ATMOS	37/39	40/36	39/36	% IIC
800	114	2	718 +/- 2	4	-	6666	30	-
850	63	1	889 +/- 2	2	-	16085	57	-
900	108	2	908 +/- 2	1	-	22904	79.5	-
950	154	3	922 +/- 2	<1	-	31982	109.3	-
975	160	3	903 +/- 2	<1	-	31177	109.3	-
1000	181	4	907 +/- 2	1	-	23587	82	-
1025	500	10	906 +/- 2	1	-	27333	95.4	-
1050	882	18	908 +/- 2	<1	-	33465	116.6	-
1075	1078	21	910 +/- 2	<1	-	46352	161.5	-
1100	770	15	905 +/- 2	<1	-	45333	159.1	-
1125	343	7	910 +/- 2	<1	-	51874	181	-
1150	255	5	909 +/- 2	<1	-	36730	128	-
1175	261	5	908 +/- 2	<1	-	38071	132.9	-
1200	166	3	908 +/- 2	<1	-	32374	112.9	-

TOTAL GAS AGE = 904 Ma

J = 2.303E-03

ERROR ESTIMATES AT ONE SIGMA LEVEL

37/39,40/36 AND 39/36 Ar RATIOS ARE CORRECTED FOR INTERFERING ISOTOPES

% IIC - INTERFERING ISOTOPES CORRECTION

Table A4.4 Analysis summary for sample 4.

DMG-N202 MUSCOVITE SUMMARY

°C	mV 39	% 39	AGE(Ma)	% ATMOS	37/39	40/36	39/36	% IIC
650	8	3	842 +/- 3	5	-	5812	21.6	-
780	13	5	903 +/- 3	2	-	14915	52.6	-
710	28	11	905 +/- 1	2	-	19962	70.6	-
740	40	16	903 +/- 1	2	0	18675	66.1	0
770	47	19	905 +/- 1	2	-	19174	67.8	-
800	30	12	903 +/- 1	3	-	10879	38.1	-
830	17	7	904 +/- 1	3	-	9394	32.7	-
860	13	5	901 +/- 2	5	-	5410	18.4	-
890	10	4	904 +/- 2	7	-	4352	14.5	-
920	9	4	907 +/- 2	8	-	3537	11.6	-
1000	22	9	904 +/- 1	6	-	4939	16.6	-
1100	12	5	901 +/- 2	22	-	1313	3.6	-
1140	1	<1	747 +/- 144	85	-	348	.2	-

TOTAL GAS AGE = 901 Ma

J = 2.34E-03

ERROR ESTIMATES AT ONE SIGMA LEVEL

37/39,40/36 AND 39/36 Ar RATIOS ARE CORRECTED FOR INTERFERING ISOTOPES

% IIC - INTERFERING ISOTOPES CORRECTION

Table A4.5 Analysis summary for sample 5.

HLK RD MUSCOVITE SUMMARY

°C	mV 39	% 39	AGE (Ma)	% ATMOS	37/39	40/36	39/36	% IIC
650	8	5	843 +/- 4	6	-	4978	18.3	-
680	10	6	889 +/- 3	4	-	8228	29.1	-
710	30	19	899 +/- 1	2	-	15745	55.9	-
740	27	16	898 +/- 1	2	-	13402	47.5	-
770	24	15	900 +/- 1	3	-	10252	36	-
800	21	13	897 +/- 1	4	-	7499	26.1	-
830	17	10	902 +/- 1	6	-	5170	17.5	-
860	10	6	905 +/- 2	11	-	2715	8.6	-
890	6	3	898 +/- 7	22	-	1361	3.8	-
920	4	2	888 +/- 9	37	-	791	1.8	-
1000	5	3	885 +/- 8	50	-	596	1.1	-

TOTAL GAS AGE = 895 Ma

J = 2.34E-03

ERROR ESTIMATES AT ONE SIGMA LEVEL

37/39,40/36 AND 39/36 Ar RATIOS ARE CORRECTED FOR INTERFERING ISOTOPES

% IIC - INTERFERING ISOTOPES CORRECTION

Table A4.6 Analysis summary for sample 6.

NC90-529A MUSCOVITE SUMMARY

°C	mV 39	% 39	AGE(Ma)	% ATMOS	37/39	40/36	39/36	% IIC
650	46	12	796 +/- 1	4	-	7896	32	-
680	18	5	854 +/- 2	4	-	6776	25	-
710	31	8	872 +/- 1	4	-	8442	30.6	-
740	69	18	890 +/- 2	3	-	9699	34.5	-
770	47	12	894 +/- 3	3	-	9284	32.8	-
800	24	6	893 +/- 2	5	-	6487	22.6	-
830	47	12	895 +/- 1	6	-	4990	17	-
860	34	9	896 +/- 1	12	-	2475	7.9	-
890	13	3	904 +/- 2	18	-	1617	4.7	-
930	10	3	900 +/- 3	25	-	1198	3.2	-
1000	27	7	908 +/- 1	21	-	1395	3.9	-
1100	27	7	909 +/- 2	36	-	823	1.8	-

TOTAL GAS AGE = 881 Ma

J = 2.34E-03

ERROR ESTIMATES AT ONE SIGMA LEVEL

37/39,40/36 AND 39/36 Ar RATIOS ARE CORRECTED FOR INTERFERING ISOTOPES

% IIC - INTERFERING ISOTOPES CORRECTION

Table A4.7 Analysis summary for sample 7.

NC90-193A MUSCOVITE SUMMARY

°C	mV 39	% 39	AGE(Ma)	% ATMOS	37/39	40/36	39/36	% IIC
600	12	2	758 +/- 4	21	-	1420	5	-
650	9	1	863 +/- 5	11	-	2760	9.4	-
680	13	2	891 +/- 3	9	-	3229	10.7	-
710	60	9	900 +/- 1	3	-	9142	31.9	-
740	96	15	903 +/- 1	2	-	18143	64.2	-
770	121	19	894 +/- 2	2	-	12868	45.8	-
810	85	13	889 +/- 2	3	-	10852	38.8	-
840	67	10	896 +/- 5	2	-	12701	45.1	-
870	35	5	884 +/- 4	5	-	6166	21.7	-
900	22	3	901 +/- 2	4	-	7779	27	-
930	23	4	898 +/- 2	5	-	5800	19.9	-
1000	51	8	898 +/- 2	4	-	8173	28.5	-
1050	52	8	902 +/- 2	5	-	6344	21.8	-

TOTAL GAS AGE = 893 Ma

J = 2.34E-03

ERROR ESTIMATES AT ONE SIGMA LEVEL

37/39,40/36 AND 39/36 Ar RATIOS ARE CORRECTED FOR INTERFERING ISOTOPES

% IIC - INTERFERING ISOTOPES CORRECTION

Table A4.8 Analysis summary for sample 8.

N428-87 MUSCOVITE SUMMARY

°C	mV 39	% 39	AGE(Ma)	% ATMOS	37/39	40/36	39/36	% IIC
650	32	4	833 +/- 1	7	-	3981	15.6	-
700	275	33	901 +/- 1	1	-	22600	85.9	-
750	267	32	904 +/- 1	1	-	27467	104.2	-
780	115	14	909 +/- 1	<1	-	38597	145.9	-
810	33	4	902 +/- 1	2	-	16560	62.5	-
840	15	2	897 +/- 2	4	-	7059	26.2	-
870	16	2	894 +/- 2	5	.1	5513	20.2	0
900	11	1	888 +/- 2	7	-	3982	14.4	-
930	53	6	906 +/- 2	10	-	2982	10.2	-
960	12	1	905 +/- 3	12	-	2451	8.2	-
990	8	1	895 +/- 3	23	-	1259	3.7	-
1050	5	<1	870 +/- 12	45	-	655	1.4	-

TOTAL GAS AGE = 900 Ma

J = 2.495E-03

ERROR ESTIMATES AT ONE SIGMA LEVEL

37/39,40/36 AND 39/36 Ar RATIOS ARE CORRECTED FOR INTERFERING ISOTOPES

% IIC - INTERFERING ISOTOPES CORRECTION

Table A4.9 Analysis summary for sample 9.

DMG-P196-87 MUSCOVITE SUMMARY

°C	mV 39	% 39	AGE (Ma)	% ATMOS	37/39	40/36	39/36	% IIC
850	8	<1	798 +/- 3	10	-	3038	11.3	-
900	78	1	874 +/- 2	3	-	10806	38.8	-
975	71	1	903 +/- 2	<1	-	130554	461.9	-
1000	261	4	893 +/- 2	2	-	13561	47.6	-
1025	361	5	889 +/- 2	2	-	18079	64.3	-
1050	868	12	893 +/- 2	1	-	22733	80.6	-
1075	1288	18	891 +/- 2	<1	-	33369	119.1	-
1100	826	12	893 +/- 2	<1	-	40828	145.6	-
1125	686	10	894 +/- 2	<1	-	40340	143.6	-
1150	490	7	889 +/- 2	<1	-	31463	112.7	-
1175	350	5	893 +/- 2	1	-	21914	77.6	-
1200	294	4	895 +/- 2	1	-	19925	70.3	-
1225	308	4	897 +/- 2	1	-	20525	72.3	-
1250	560	8	900 +/- 2	1	-	26383	92.8	-
1275	588	8	903 +/- 2	<1	-	32640	114.6	-

TOTAL GAS AGE = 894 Ma

J = 2.303E-03

ERROR ESTIMATES AT ONE SIGMA LEVEL

37/39,40/36 AND 39/36 Ar RATIOS ARE CORRECTED FOR INTERFERING ISOTOPES

Table A4.10 Analysis summary for sample 10.

NC90-210 MUSCOVITE SUMMARY

°C	mV 39	% 39	AGE (Ma)	% ATMOS	37/39	40/36	39/36	% IIC
650	15	3	844 +/- 2	5	-	6325	23.6	-
680	31	7	894 +/- 1	2	-	13688	48.8	-
710	75	16	899 +/- 2	2	-	17378	61.8	-
740	70	15	901 +/- 2	1	-	21228	75.5	-
770	66	14	903 +/- 2	1	-	22443	79.8	-
800	44	10	903 +/- 4	1	-	22028	78.2	-
830	28	6	904 +/- 11	3	-	8524	29.5	-
860	23	5	879 +/- 12	6	-	5008	17.5	-
890	29	6	897 +/- 1	5	-	5777	19.9	-
920	36	8	898 +/- 1	5	-	5887	20.2	-
950	30	7	897 +/- 2	8	-	3876	13	-
1000	12	3	888 +/- 3	22	-	1368	3.9	-

TOTAL GAS AGE = 897 Ma

J = 2.34E-03

ERROR ESTIMATES AT ONE SIGMA LEVEL

37/39, 40/36 AND 39/36 Ar RATIOS ARE CORRECTED FOR INTERFERING ISOTOPES

% IIC - INTERFERING ISOTOPES CORRECTION

Table A4.11 Analysis summary for sample 11.

DMG-SH7A-87 MUSCOVITE SUMMARY

°C	mV 39	% 39	AGE (Ma)	% ATMOS	37/39	40/36	39/36	% IIC
700	1	<1	704 +/- 14	17	-	1718	6.7	-
900	8	<1	860 +/- 4	2	-	13112	47.7	-
950	140	2	882 +/- 2	2	-	16460	58.3	-
975	126	2	887 +/- 2	2	-	18609	65.6	-
1000	168	3	878 +/- 2	2	-	16563	58.9	-
1025	434	7	887 +/- 2	1	-	23959	84.7	-
1050	756	12	886 +/- 2	<1	-	30347	107.8	-
1075	868	14	880 +/- 2	<1	-	45131	162.3	-
1100	2114	33	884 +/- 10	2	-	16315	58.3	-
1125	924	15	884 +/- 2	<1	-	35444	126.5	-
1150	364	6	887 +/- 2	<1	-	34402	122.1	-
1175	238	4	889 +/- 2	1	-	28316	100	-
1200	224	4	883 +/- 2	1	-	24399	86.7	-

TOTAL GAS AGE = 881 Ma

J = 2.275E-03

ERROR ESTIMATES AT ONE SIGMA LEVEL

37/39, 40/36 AND 39/36 Ar RATIOS ARE CORRECTED FOR INTERFERING ISOTOPES

% IIC - INTERFERING ISOTOPES CORRECTION

Table A4.12 Analysis summary for sample 12.

DMG-NB160-88 MUSCOVITE SUMMARY

°C	mV 39	% 39	AGE(Ma)	% ATMOS	37/39	40/36	39/36	% IIC
850	112	2	829 +/- 2	5	-	6521	24.2	-
900	96	2	891 +/- 2	2	-	13767	47.9	-
950	179	4	891 +/- 2	3	-	11247	39	-
975	119	2	890 +/- 2	2	-	14822	51.8	-
1000	168	4	883 +/- 2	2	-	19320	68.5	-
1025	560	12	887 +/- 2	2	-	17295	60.9	-
1050	1176	25	901 +/- 3	<1	-	380478	1335.2	-
1075	1618	34	891 +/- 2	<1	-	68270	242.2	-
1100	771	16	884 +/- 2	2	-	19347	68.5	-

TOTAL GAS AGE = 890 Ma

J = 2.275E-03

ERROR ESTIMATES AT ONE SIGMA LEVEL

37/39,40/36 AND 39/36 Ar RATIOS ARE CORRECTED FOR INTERFERING ISOTOPES

% IIC - INTERFERING ISOTOPES CORRECTION

Table A4.13 Analysis summary for sample 13.

NB-397 MUSCOVITE SUMMARY

°C	mV 39	% 39	AGE(Ma)	% ATMOS	37/39	40/36	39/36	% IIC
650	23	4	856 +/- 1	4	-	6699	26.2	-
680	8	1	889 +/- 2	5	-	6561	24.5	-
710	13	2	902 +/- 2	2	-	13999	52.6	-
740	75	13	906 +/- 2	2	-	17116	64.3	-
770	102	18	905 +/- 1	<1	-	41691	158.4	-
800	20	4	901 +/- 1	<1	-	32656	124.5	-
830	93	17	905 +/- 1	1	-	23145	87.4	-
860	88	16	910 +/- 5	<1	-	34376	129.5	-
890	24	4	902 +/- 1	2	-	17585	66.4	-
920	18	3	901 +/- 1	2	-	12094	45.4	-
950	25	4	901 +/- 1	3	-	8886	33	-
1000	40	7	901 +/- 3	6	-	4811	17.3	-
1150	29	5	899 +/- 1	7	-	3966	14.1	-

TOTAL GAS AGE = 903 Ma

J = 2.495E-03

ERROR ESTIMATES AT ONE SIGMA LEVEL

37/39,40/36 AND 39/36 Ar RATIOS ARE CORRECTED FOR INTERFERING ISOTOPES

% IIC - INTERFERING ISOTOPES CORRECTION

Table A4.14 Analysis summary for sample 14.

APPENDIX 5: MINERAL SPECTRA

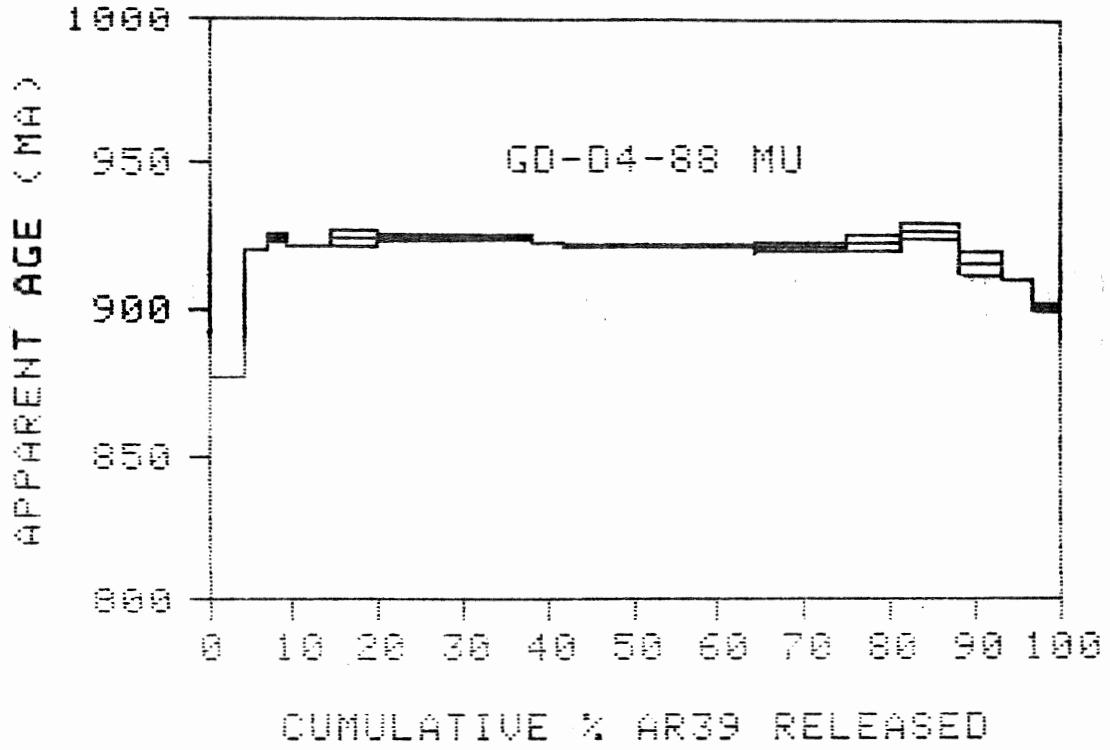

Figure A5.1 Mineral spectrum for sample 1.

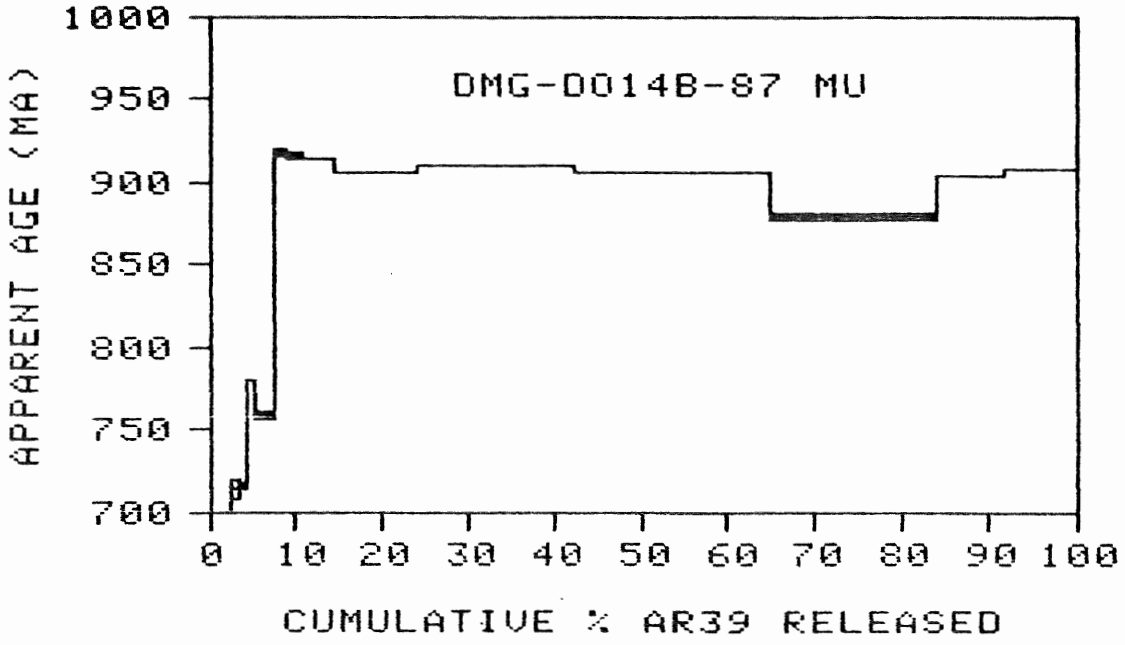

Figure A5.2 Mineral spectrum for sample 2.

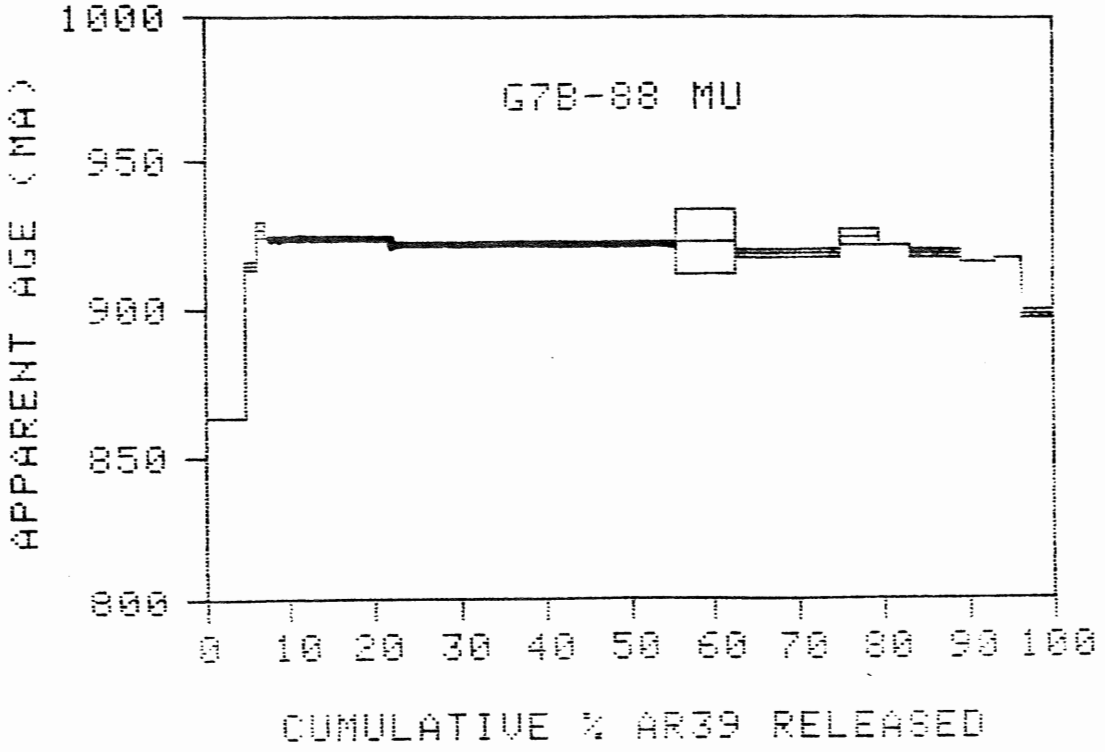

Figure A5.3 Mineral spectrum for sample 3.

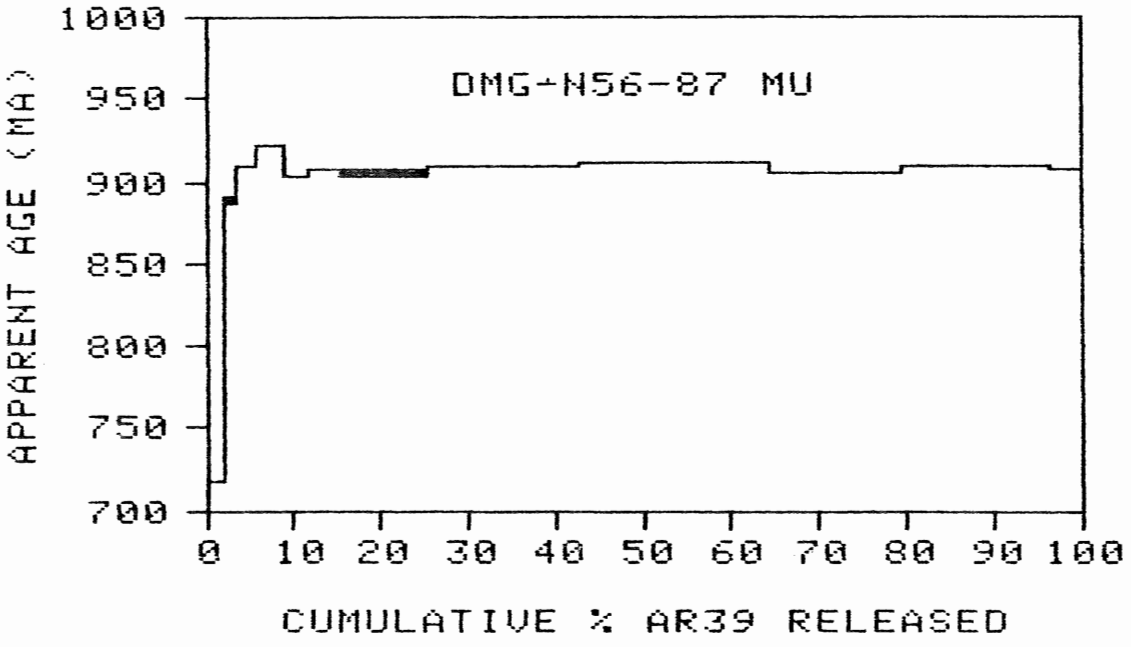

Figure A5.4 Mineral spectrum for sample 4.

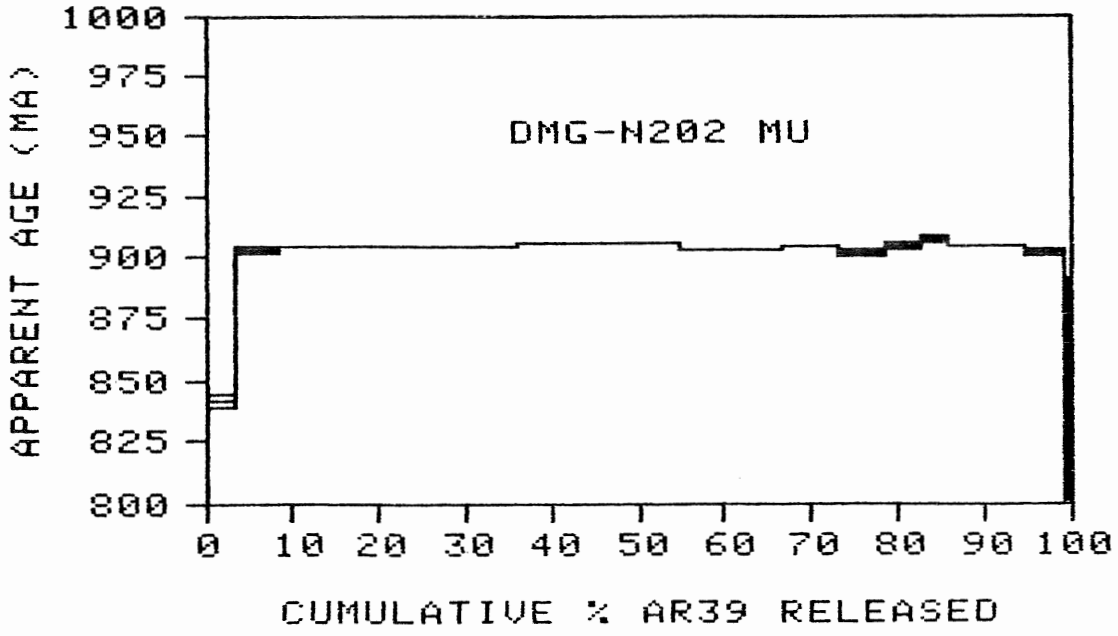

Figure A5.5 Mineral spectrum for sample 5.

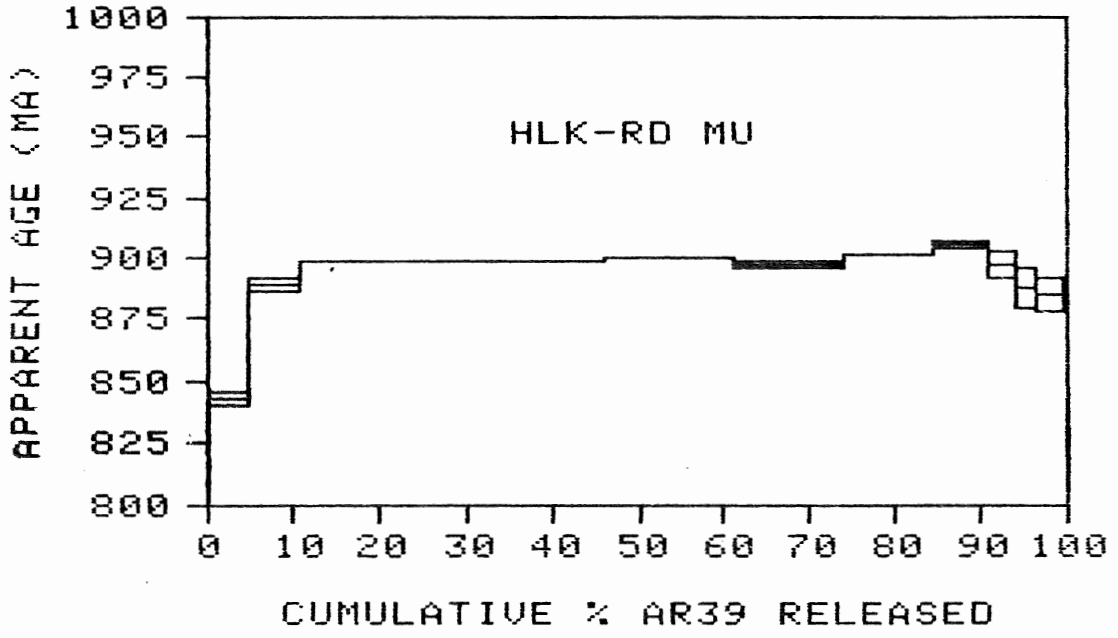

Figure A5.6 Mineral spectrum for sample 6.

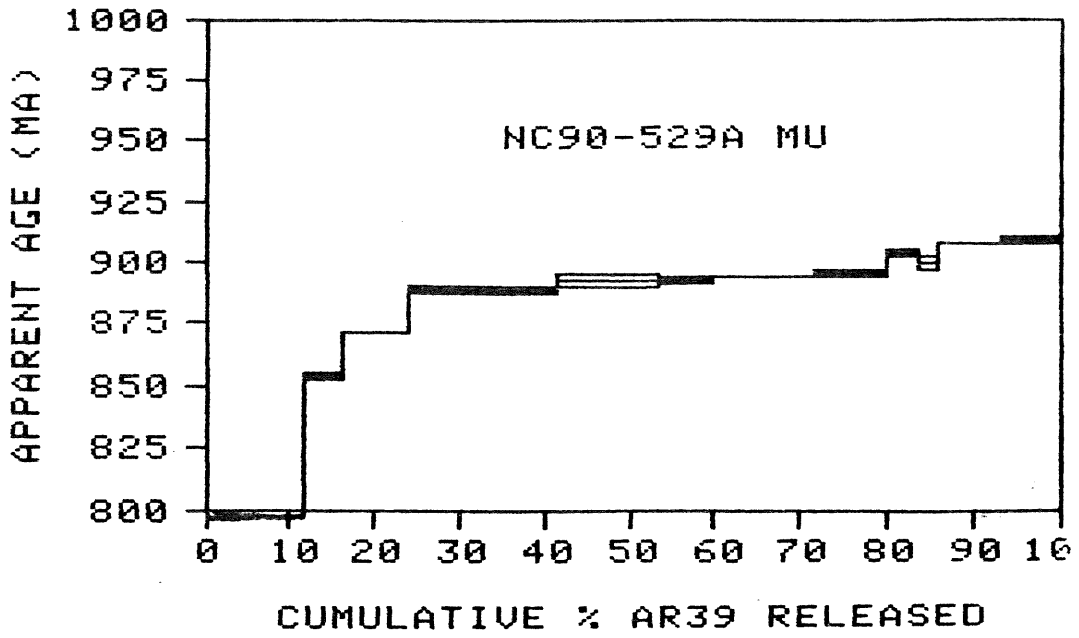

Figure A5.7 Mineral spectrum for sample 7.

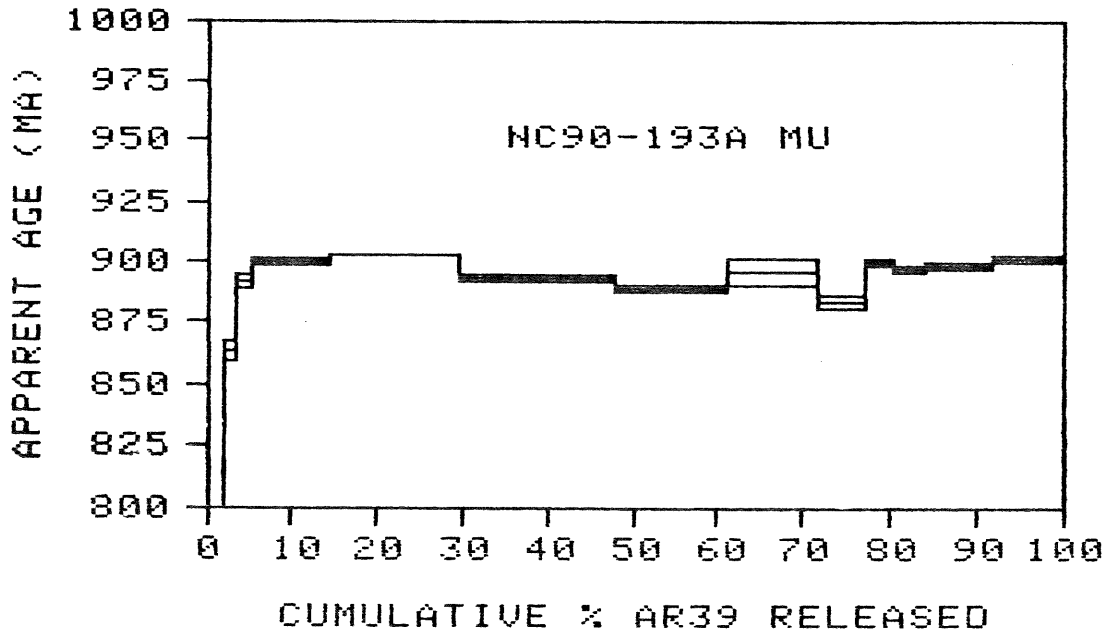

Figure A5.8 Mineral spectrum for sample 8.

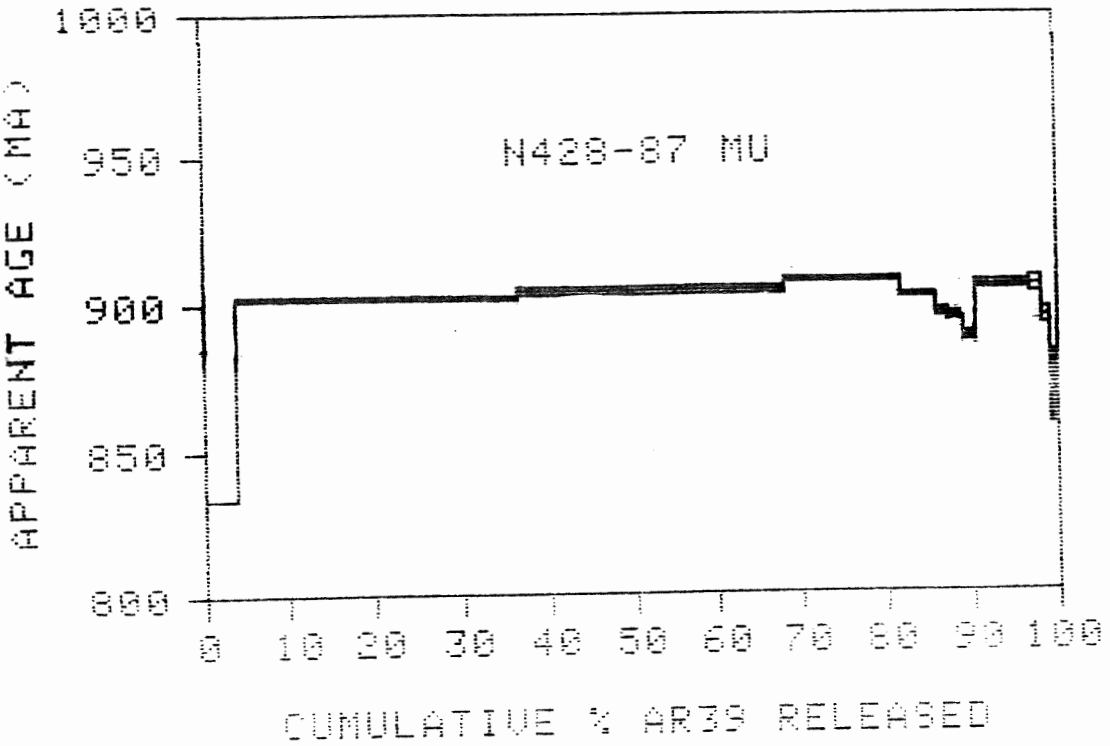

Figure A5.9 Mineral spectrum for sample 9.

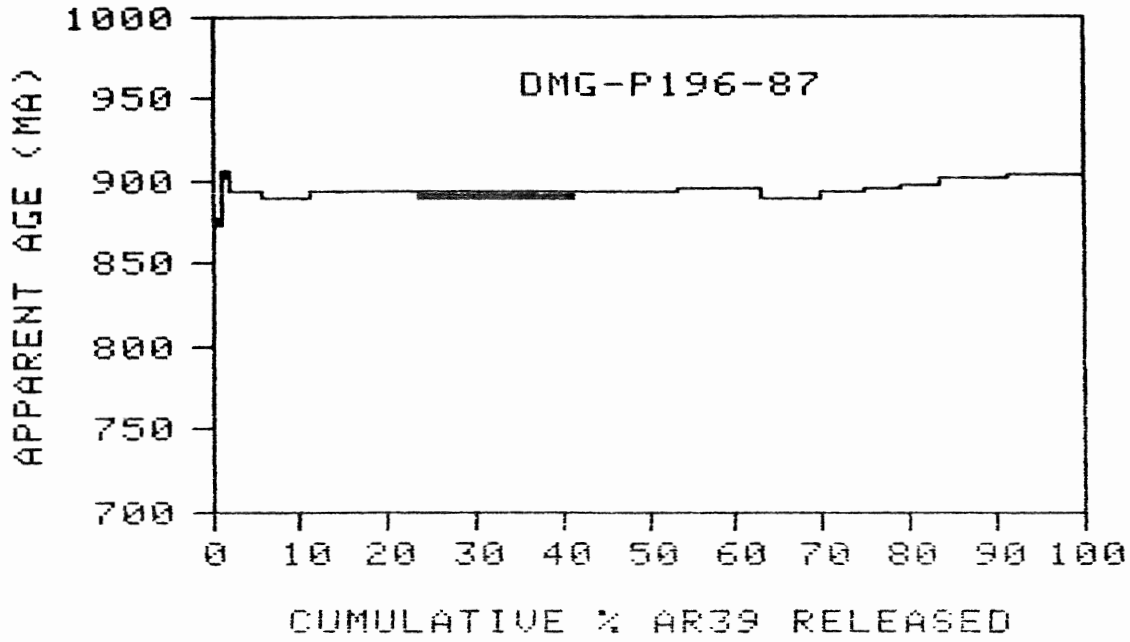

Figure A5.10 Mineral spectrum for sample 10.

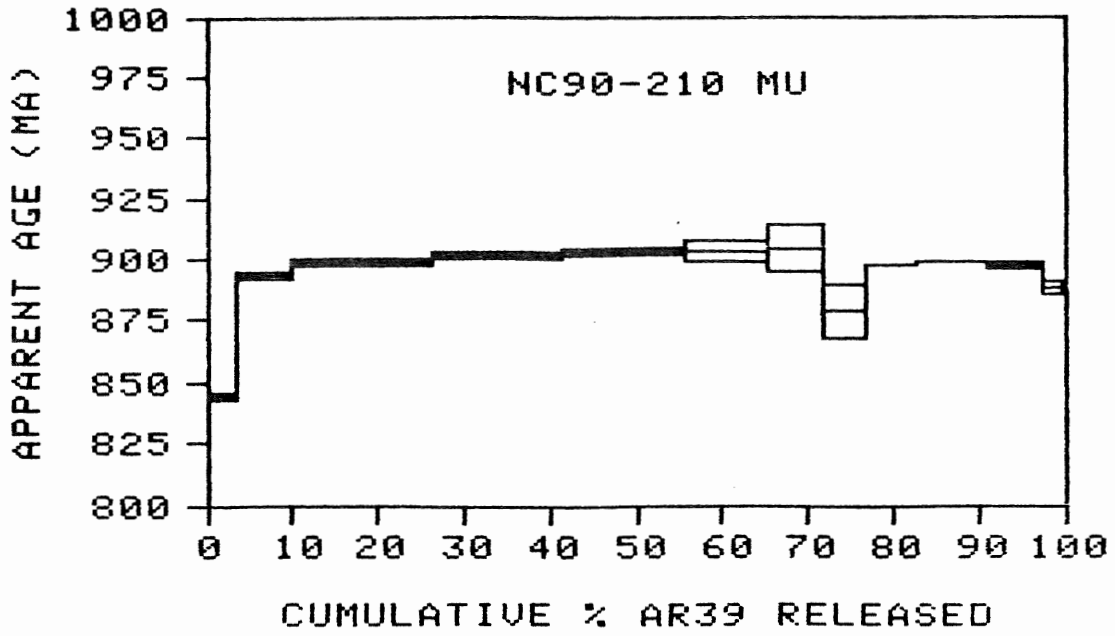

Figure A5.11 Mineral spectrum for sample 11.

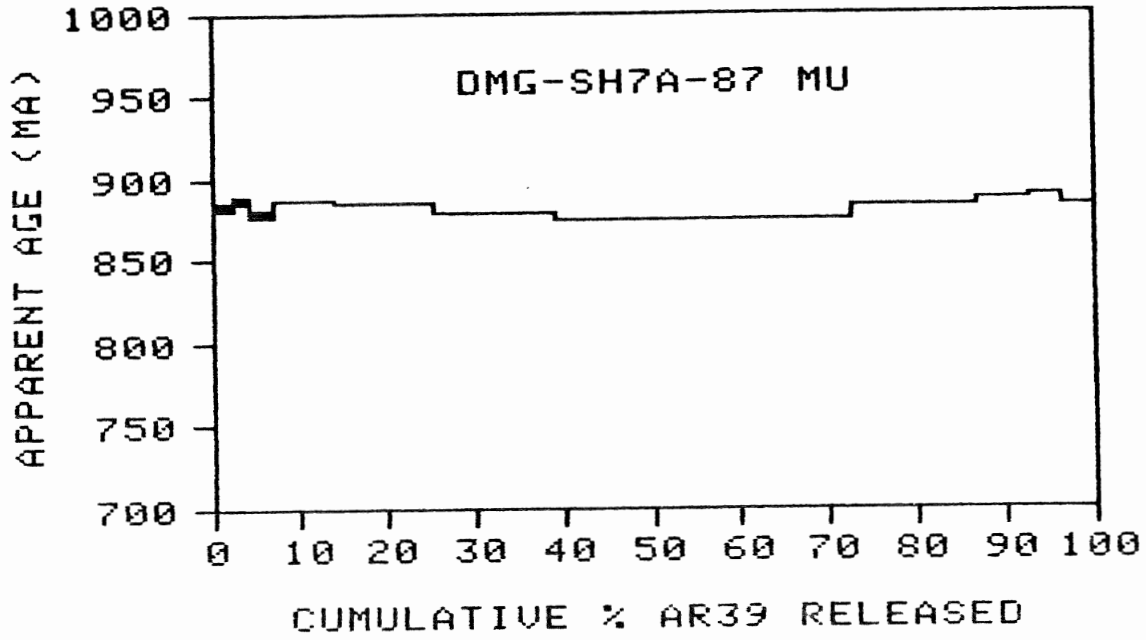

Figure A5.12 Mineral spectrum for sample 12.

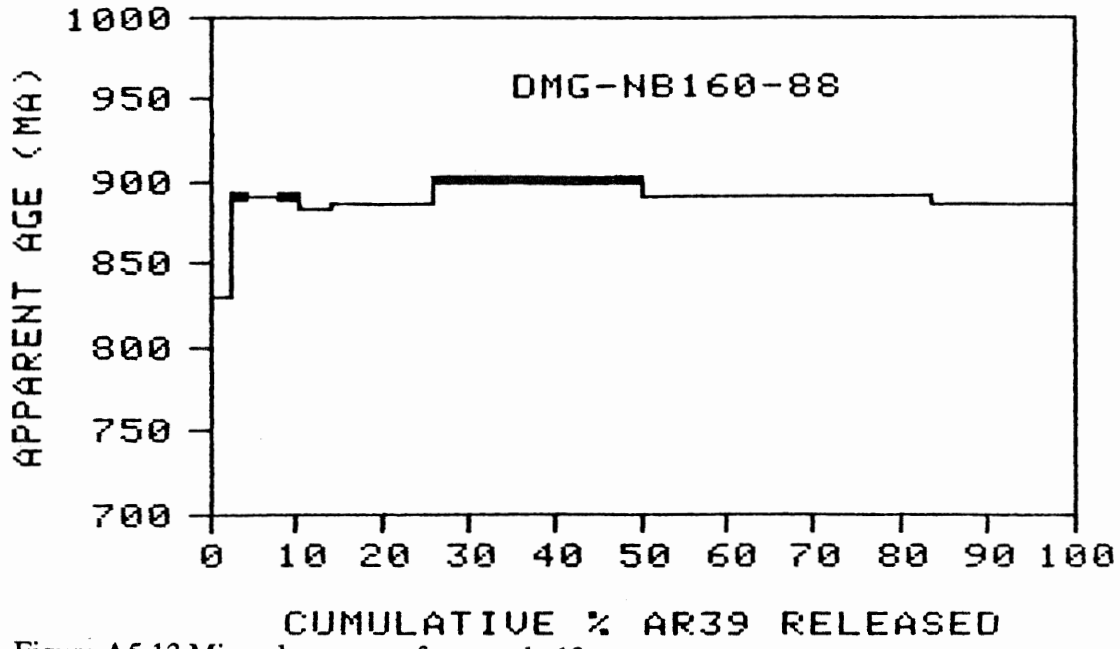

Figure A5.13 Mineral spectrum for sample 13.

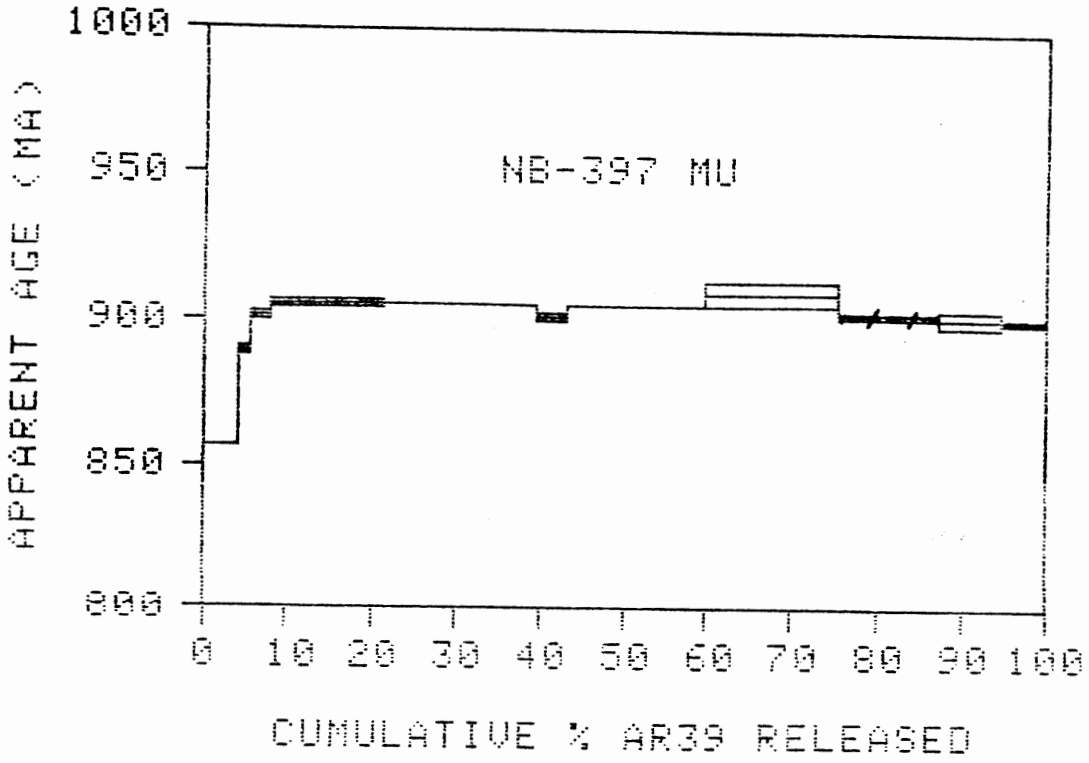

Figure A5.14 Mineral spectrum for sample 14.

APPENDIX 6: SAMPLE CALCULATIONS

Ages of samples were calculated by the plateau method, where possible, as described by Fleck et al. (1977). This method was used for samples 1, 3, 4, 5, 6, 9, 10, 11, 12, and 14.

An example of these calculations is provided for sample 4. The critical value was calculated as

$$C.V. = 1.960\ (\sigma_1^2 + \sigma_2^2)^{1/2}$$
$$= 1.960\ (2^2 + 2^2)^{1/2}$$
$$= 5.5$$

Determination of this value lead to the identification of nine steps to be used in the age calculation.

$$t = \frac{(4 * 907) + (10 * 906) + (18 * 908) + (21 * 910) + (15 * 905) + (7 * 910) + (5 * 909) + (5 * 908) + (3 * 908)}{(4+10+18+21+15+7+5+5+3)}$$

$$= 79896 / 88$$
$$= 907.91$$

The calculated age of this sample is 908 Ma. Figure A6.1 is its spectrum, with the plateau marked.

The J value of this sample is 0.00234 ± 0.00001. As a percentage of the total, the error may be expressed as

$$0.00001 / 0.00234 = 0.00427$$
$$= 0.427\%$$

0.427% of the age is then calculated to determine the error in the age

$$\sigma t = 907.91 * 0.00427$$
$$= 3.88$$

Therefore, the age of the sample, including its error, is 907 ± 4 Ma.

As discussed in section 5.2, several of the ages were recalculated. These recalculations are displayed in Table A6.1 and explained here. The calculated average of the ages from the earlier set is 913.48 Ma while the calculated average of the trusted ages from this study (all of the remaining ones, except sample 7 because of its argon loss) is 897.99 Ma. The difference in averages, 15.48 Ma, has been subtracted from each age of the earlier set. The new values, along with the trusted ones, have been tabled as Adjusted Ages. These ages are the ones used in the remainder of this study.

Apparent Ages:	Culshaw's Ages:	New Ages:	Recalula-ted Ages:	Adjusted Ages:
923.55	923.55		908.07	907.06
906.06		906.06		906.06
922.10	922.10		906.62	905.61
907.91		907.91		907.91
904.03		904.03		904.03
898.57		898.57		898.57
893.16				
896.30		896.30		896.30
903.55	903.55		888.07	887.06
892.14		892.14		892.14
901.29		901.29		901.29
884.08		884.08		884.08
891.57		891.57		891.57
904.71	904.71		889.23	888.22
totals	3653.91	8081.95		
average	913.48	897.99		
difference of averages		15.48		

Table A6.1 Apparent Ages to Adjusted Ages. All ages are in Ma. Apparent Ages are those of Table 5.1. Culshaw's Ages are those from Culshaw et al. (1990). New Ages are those determined from from plateaus in this study. Recalculated Ages are Culshaw's Ages recalculated. Adjusted Ages are the final ages used in this study. The seventh value was discounted because its spectrum showed the pattern of argon loss. See text for further explanation.

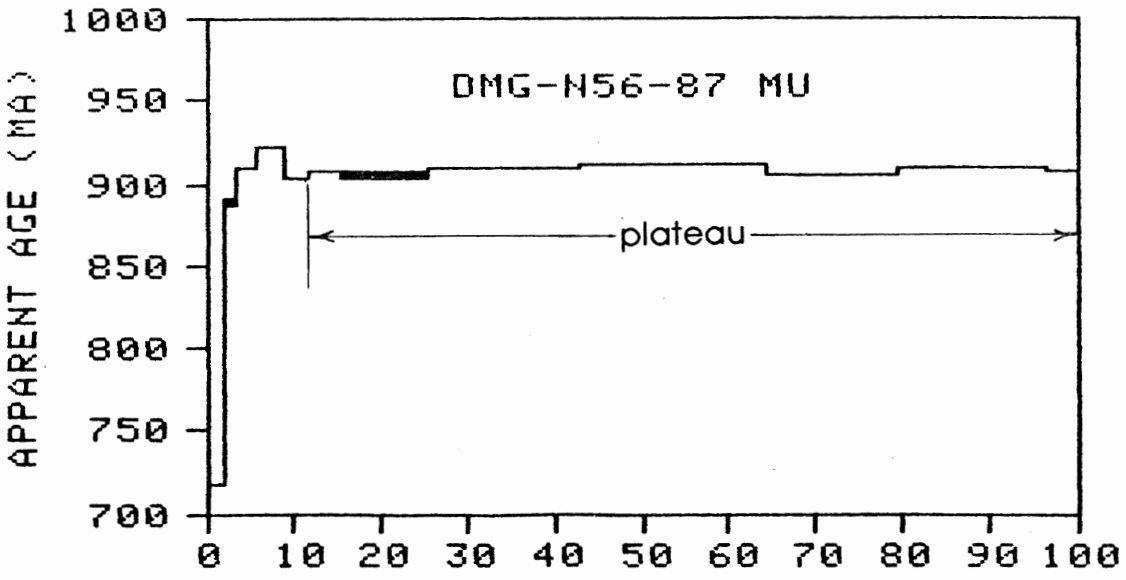

Figure A6.1 Spectrum of sample 4, with plateau marked.

APPENDIX 7: DETAILS OF MODELING PROGRAM (1DT)

Table 1.7 outlines the parameters used in the one-dimensional thermal model of the Britt Domain by Culshaw et al. (1990). Figures A7.1 and A7.2 show the depth-time plot and temperature-time plot, respectively, of this model.

Figures A7.3 through A7.8 show graphically the results of adjusting the en-bloc velocity of stage 3 (boxed) to make the temperature-time paths pass through various points of the muscovite box. Note that the scales of these plots are different than the scales of the first two plots.

Figure A7.9 is a model of Gaudemer et al. (1988) from which different geothermal gradients were calculated. Shortening rate is 5 mm / a and width is 300 km. Each vertical line corresponds to the location of one end of the transect line. Table A7.2 lists the geothermal gradients estimated.

Use of these two geothermal gradients allowed 1DT to produce two temperature-time paths (Fig. 6.6). All other parameters of the model remained as in Table A7.1.

```
thermal conductivity (W m-1 K-1) = 2.00E+00
density (kg m-3) = 2.78E+03     heat capacity (J K-1 kg-1) = 9.00E+02

# layers = 3     # stages in uplift history = 5

total model time (years) = 5.000E+08

surface temperature = 0 C;  initial basal flux (W m-2) = 3.00E-02
constant basal flux

Heat generation in the modelled space:
--surface------------------------------------- Z = 0.00 km --
LAYER 1     heat generation at  top of layer = 2.00E-06 W m-3
            heat generation at base of layer = 2.00E-06 W m-3
------------------------------------------------ Z =15.00 km --
LAYER 2     heat generation at  top of layer = 0.00E+00 W m-3
            heat generation at base of layer = 0.00E+00 W m-3
------------------------------------------------ Z =18.00 km --
LAYER 3     heat generation at  top of layer = 2.00E-06 W m-3
            heat generation at base of layer = 2.00E-06 W m-3
------------------------------------------------ Z =33.00 km --
                              heat generation = 0.0
Initial surface flux =    0.00 W m-2

Prescribed initial gradient

Velocities relative to the earth's surface (negative values for uplift):
         time at end of  en-bloc velocity  strain rate  "thrust" event
         stage, in yrs      in mm/yr          in sec-1      (Y or N)
Stage 1     5.00E+06         -0.50          -1.0E-15          N
Stage 2     7.50E+07         -0.11          0.00E+00          N
Stage 3     1.55E+08         -0.10          0.00E+00          N
Stage 4     2.35E+08         -0.05          0.00E+00          N
Stage 5     4.35E+08         -0.03          0.00E+00          N

                  time        thickness of        amount of section
                  years     thrust sheet (km)       duplicated (km)

time-step (years) = 5.00E+04
# of depth steps = 65   depth-step size (km) =  1.00
model depth (km) =  65.00

P-T-t data recorded every 1 timesteps
    5 timesteps between plots of the geotherm
P-T paths tracked for 3 points:
          point 1       initial depth (km) = 10.00
          point 2       initial depth (km) = 20.00
          point 3       initial depth (km) = 30.00
```

Table A7.1 Parameters of model of Culshaw et al. (1990).

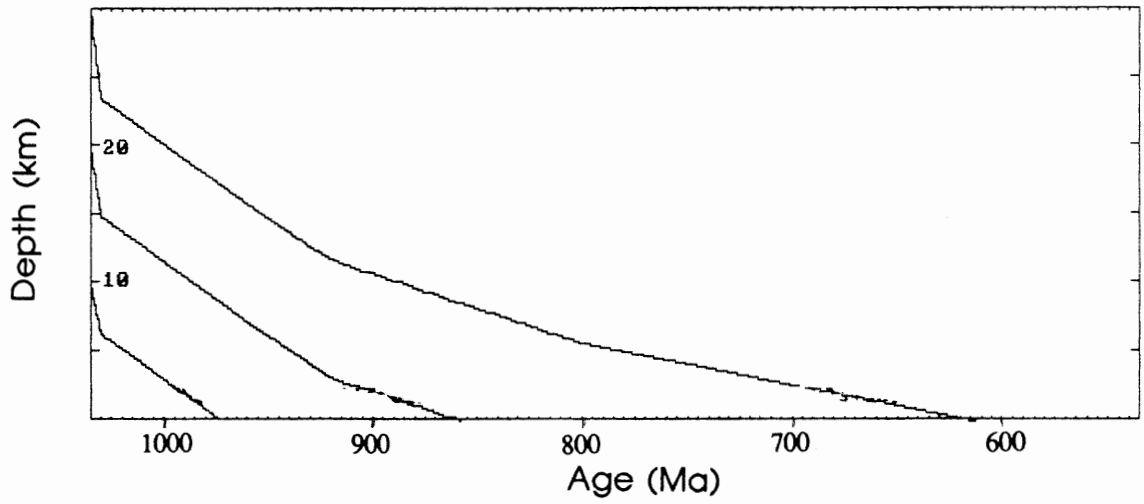

Figure A7.1 Depth-time plot of uplift history of three points originating at 10, 20, and 30 km depth, according to model of Culshaw et al. (1990). Numbers indicate stages of uplift.

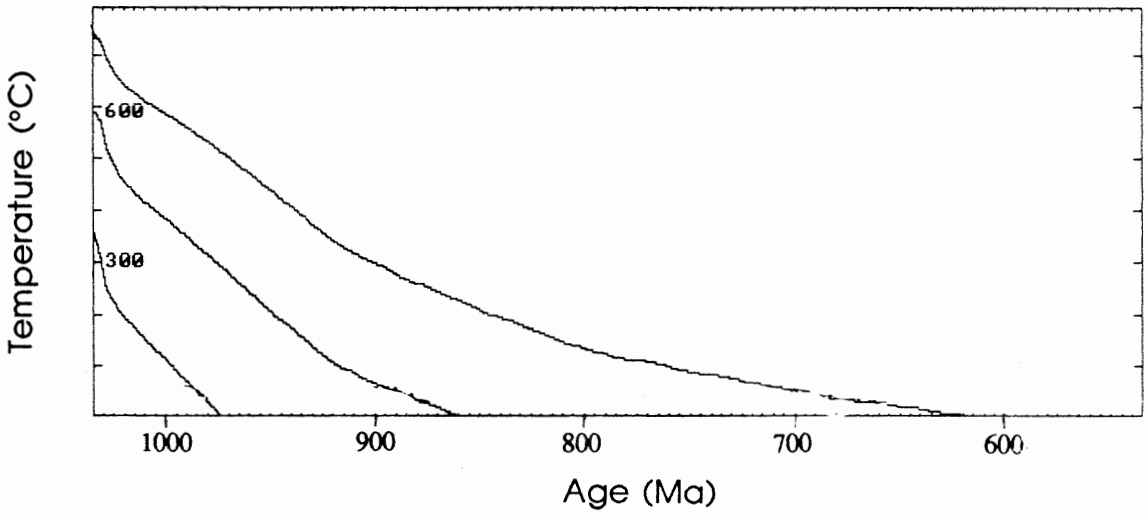

Figure A7.2 Temperature-time plot of uplift history of three points originating at 10, 20, and 30 km depth, according to model of Culshaw et al. (1990). Numbers indicate stages of uplift.

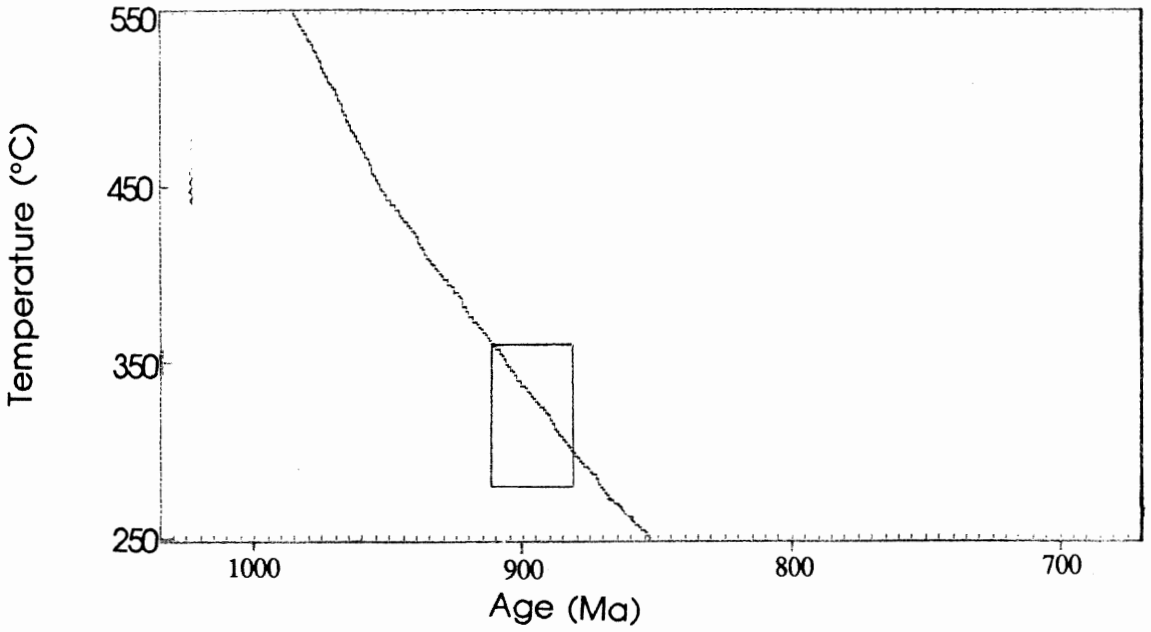

Figure A7.3 Temperature-time path which intersects northernmost sample at maximum closure temperature. Rate of uplift for stage 3 is 0.06 mm / year.

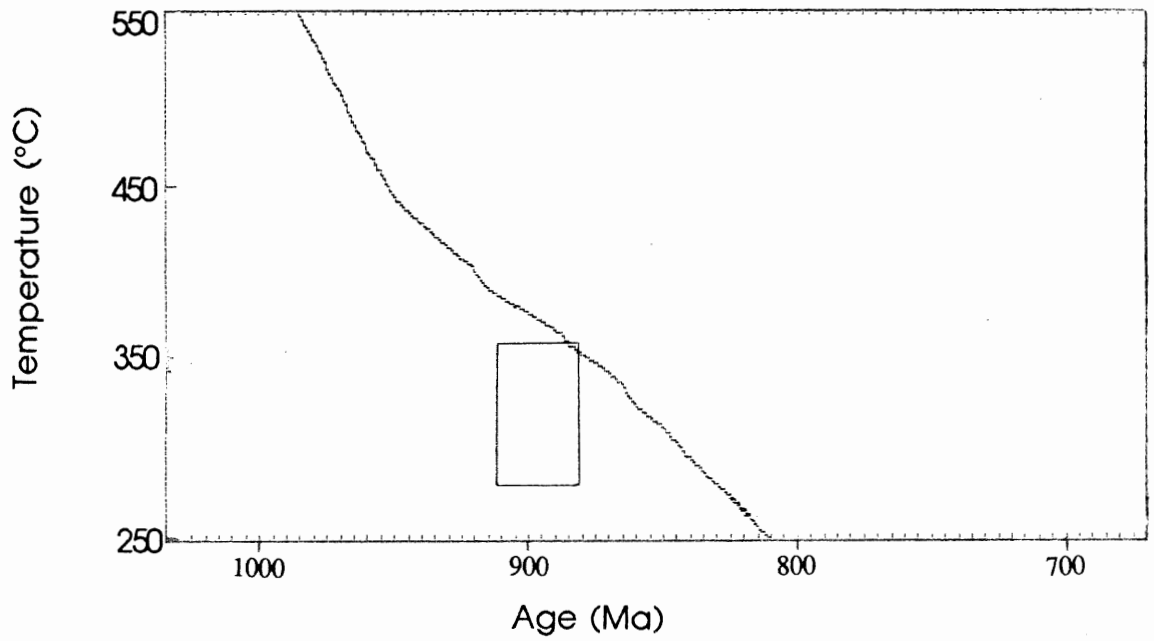

Figure A7.4 Temperature-time path which intersects southernmost sample at maximum closure temperature. Rate of uplift for stage 3 is 0.03 mm / year.

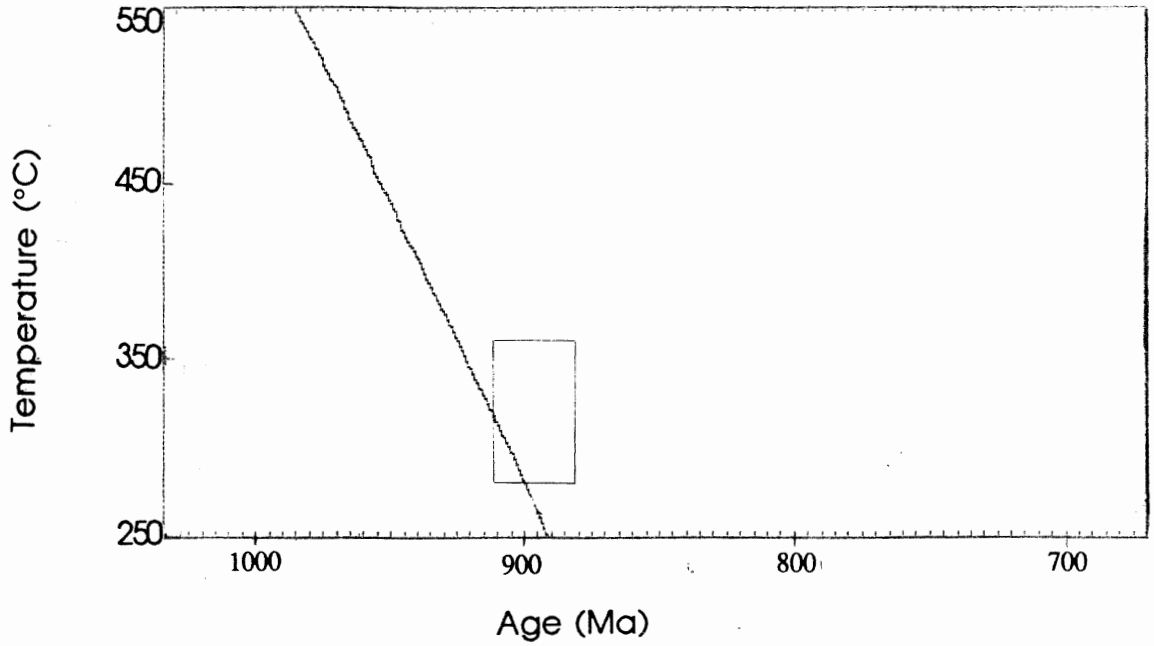

Figure A7.5 Temperature-time path which intersects northernmost sample at median closure temperature. Rate of uplift for stage 3 is 0.10 mm / year.

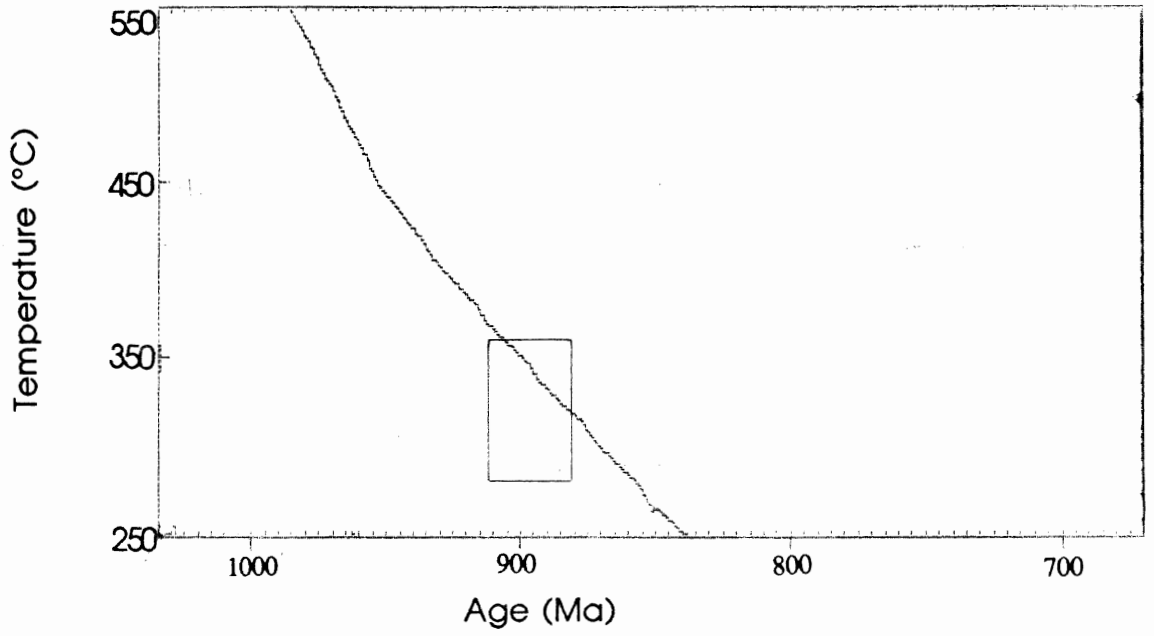

Figure A7.6 Temperature-time path which intersects southernmost sample at median closure temperature. Rate of uplift for stage 3 is 0.05 mm / year.

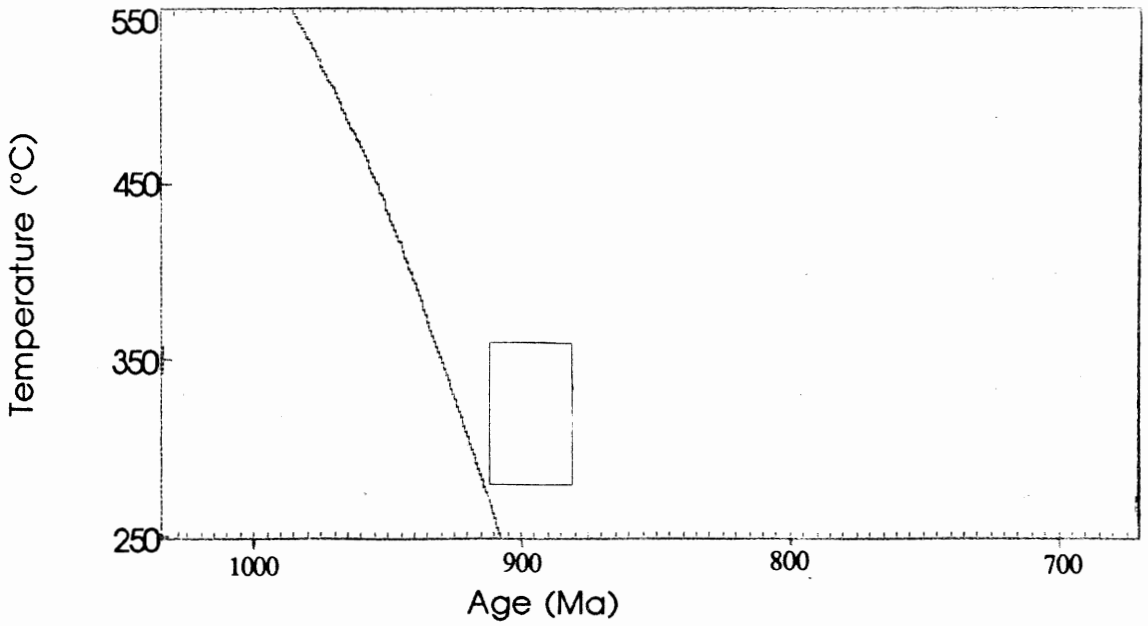

Figure A7.7 Temperature-time path which intersects northernmost sample at minimum closure temperature. Rate of uplift for stage 3 is 0.14 mm / year.

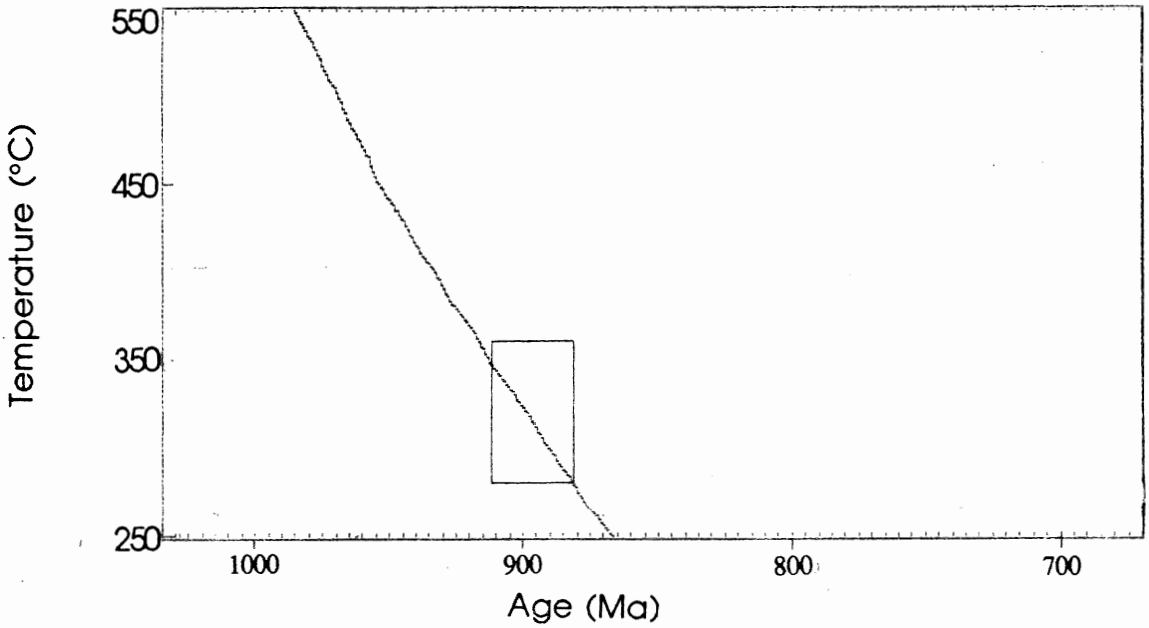

Figure A7.8 Temperature-time path which intersects southernmost sample at minimum closure temperature. Rate of uplift for stage 3 is 0.07 mm / year.

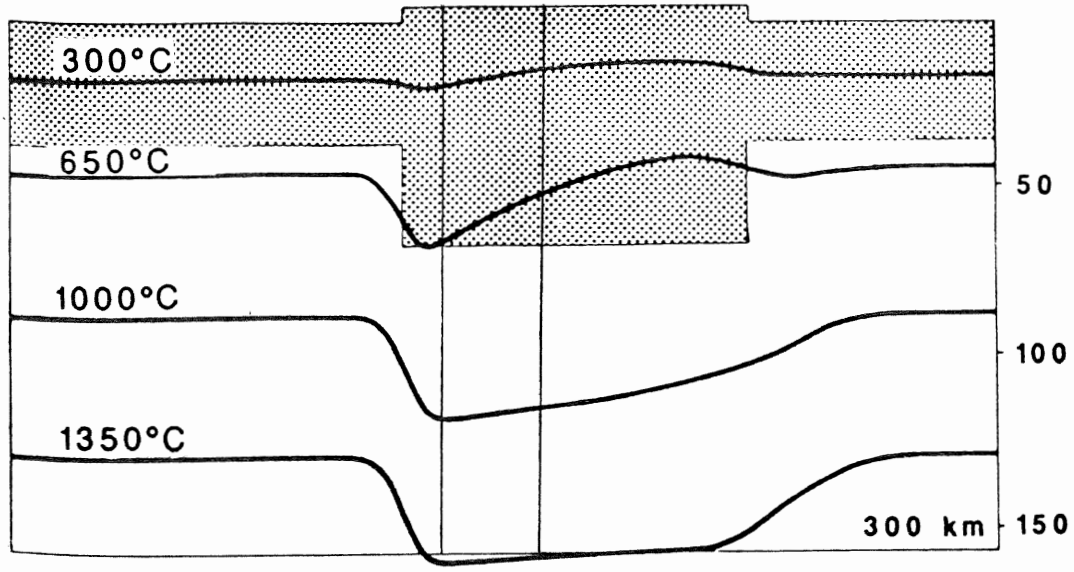

Figure A7.9 Estimation of two geothermal gradients from model of Gaudemer et al. (1988).

	Depths	
Temperature	Shallower Gradient	Steeper Gradient
300° C	24 km	19 km
650° C	70 km	57 km
1000° C	124 km	120

Table A7.2 Geothermal gradients estimated from Figure A7.9.